Cell

Mechanisms of readthrough mitigation reveal principles of GCN1-mediated translational quality control

Graphical abstract

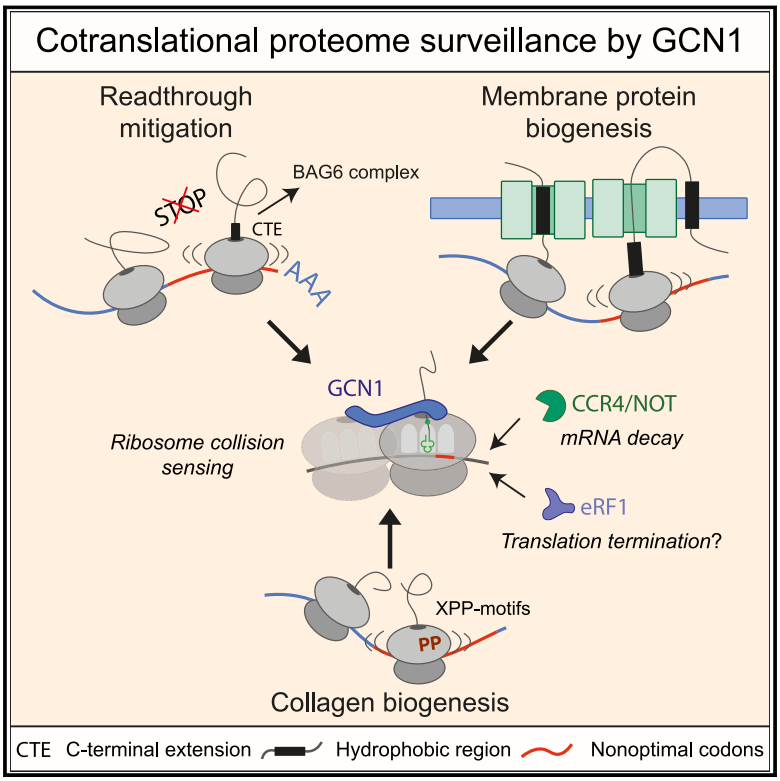

Highlights

- Hydrophobic readthrough proteins are cleared by the BAG6 complex and RNF126
- Readthrough mRNA undergoes decay mediated by GCN1 and CCR4/NOT
- GCN1 senses ribosome collisions on nonoptimal codons
- Transmembrane proteins and collagens are major targets of GCN1 surveillance

Authors

Martin B.D. Müller, Prasad Kasturi, Gopal G. Jayaraj, F. Ulrich Hartl

Correspondence

jayaraj@biochem.mpg.de (G.G.J.), uhartl@biochem.mpg.de (F.U.H.)

In brief

A ribosome-based quality control pathway coordinated by GCN1 ensures the clearance of both aberrant translation products and the associated transcripts.

Müller et al., 2023, Cell *186*, 3227–3244
July 20, 2023
https://doi.org/10.1016/j.cell.2023.05.035

CellPress

Cell

CellPress
OPEN ACCESS

Article

Mechanisms of readthrough mitigation reveal principles of GCN1-mediated translational quality control

Martin B.D. Müller,[1] Prasad Kasturi,[1,3] Gopal G. Jayaraj,[1,*] and F. Ulrich Hartl[1,2,4,*]
[1]Department of Cellular Biochemistry, Max Planck Institute of Biochemistry, Am Klopferspitz 18, 82152 Martinsried, Germany
[2]Munich Cluster for Systems Neurology (SyNergy), Munich, Germany
[3]Present address: School of Biosciences and Bioengineering, Indian Institute of Technology Mandi, Kamand, Himachal Pradesh, India
[4]Lead contact
*Correspondence: jayaraj@biochem.mpg.de (G.G.J.), uhartl@biochem.mpg.de (F.U.H.)
https://doi.org/10.1016/j.cell.2023.05.035

SUMMARY

Readthrough into the 3′ untranslated region (3′ UTR) of the mRNA results in the production of aberrant proteins. Metazoans efficiently clear readthrough proteins, but the underlying mechanisms remain unknown. Here, we show in *Caenorhabditis elegans* and mammalian cells that readthrough proteins are targeted by a coupled, two-level quality control pathway involving the BAG6 chaperone complex and the ribosome-collision-sensing protein GCN1. Readthrough proteins with hydrophobic C-terminal extensions (CTEs) are recognized by SGTA-BAG6 and ubiquitylated by RNF126 for proteasomal degradation. Additionally, cotranslational mRNA decay initiated by GCN1 and CCR4/NOT limits the accumulation of readthrough products. Unexpectedly, selective ribosome profiling uncovered a general role of GCN1 in regulating translation dynamics when ribosomes collide at nonoptimal codons, enriched in 3′ UTRs, transmembrane proteins, and collagens. GCN1 dysfunction increasingly perturbs these protein classes during aging, resulting in mRNA and proteome imbalance. Our results define GCN1 as a key factor acting during translation in maintaining protein homeostasis.

INTRODUCTION

Eukaryotic cells invest in extensive protein quality control machineries to ensure translational fidelity and prevent the accumulation of aberrant, potentially toxic proteins. Multiple transcriptional and translational surveillance mechanisms operate to maintain protein homeostasis ("proteostasis") and reduce the burden on downstream machineries of molecular chaperones and degradation systems.[1,2] A decline in proteostasis capacity, accompanied by a decrease in translation fidelity and efficiency,[3–5] is a major hallmark of aging and age-related diseases.[6–8]

A significant source of aberrant proteins arises when translational termination fails at stop codons, producing polypeptides with C-terminal extensions (CTEs) encoded by 3′ untranslated regions (3′ UTRs) of mRNAs. Readthrough is pervasive,[9] with frequencies varying from <1% to over 10%,[10] posing a sizable problem. Moreover, stop codon readthrough increases with aging, particularly in neurons.[11] Translation through 3′ UTRs into poly(A) tails of mRNAs generates ribosome-stalled nascent chains that activate the ribosome quality control (RQC) pathway.[12,13] The RQC complex recognizes translation of non-stop proteins facilitating their ubiquitylation for proteasomal degradation. Concomitantly, the non-stop mRNAs are degraded by non-stop decay involving the exosome.[14,15] However, readthrough typically does not reach the poly(A) sequence, as most transcripts contain additional termination codons in the 3′ UTR before the poly(A) tail. These nascent polypeptides are therefore not RQC substrates. Depending on the mRNA, readthrough can add hundreds of amino acids to the nascent chain. Several pathologies result from late frameshifts or stop codon mutations resulting in proteins with 3′ UTR-encoded CTEs. These aberrant proteins are either dysfunctional or may form toxic aggregates.[16–18]

Metazoans limit toxic CTE production by efficiently clearing readthrough proteins, especially when their 3′ UTRs encode hydrophobic sequences.[19] Proteolysis by the proteasome and lysosome has been implicated in degrading readthrough products.[16,20,21] Other studies suggested that ribosome queuing and translation inhibition limits CTE protein production.[22,23] Thus, the underlying clearance mechanisms and machineries involved in translation readthrough mitigation remain uncharacterized.

Here, we investigated the fate of aberrant readthrough proteins in *Caenorhabditis elegans* (*C. elegans*) and mammalian cells. We found that readthrough proteins carrying hydrophobic CTEs are cleared similarly to mistargeted tail anchored (TA) membrane proteins.[24,25] The Bcl-2-associated athanogene 6 (BAG6) chaperone complex recognizes readthrough proteins, then the E3 ligase RNF126 ubiquitylates them to enable proteasomal degradation. Our experiments further revealed that readthrough mRNAs are also efficiently degraded, defining a two-tiered quality control mechanism. We identified the ribosome

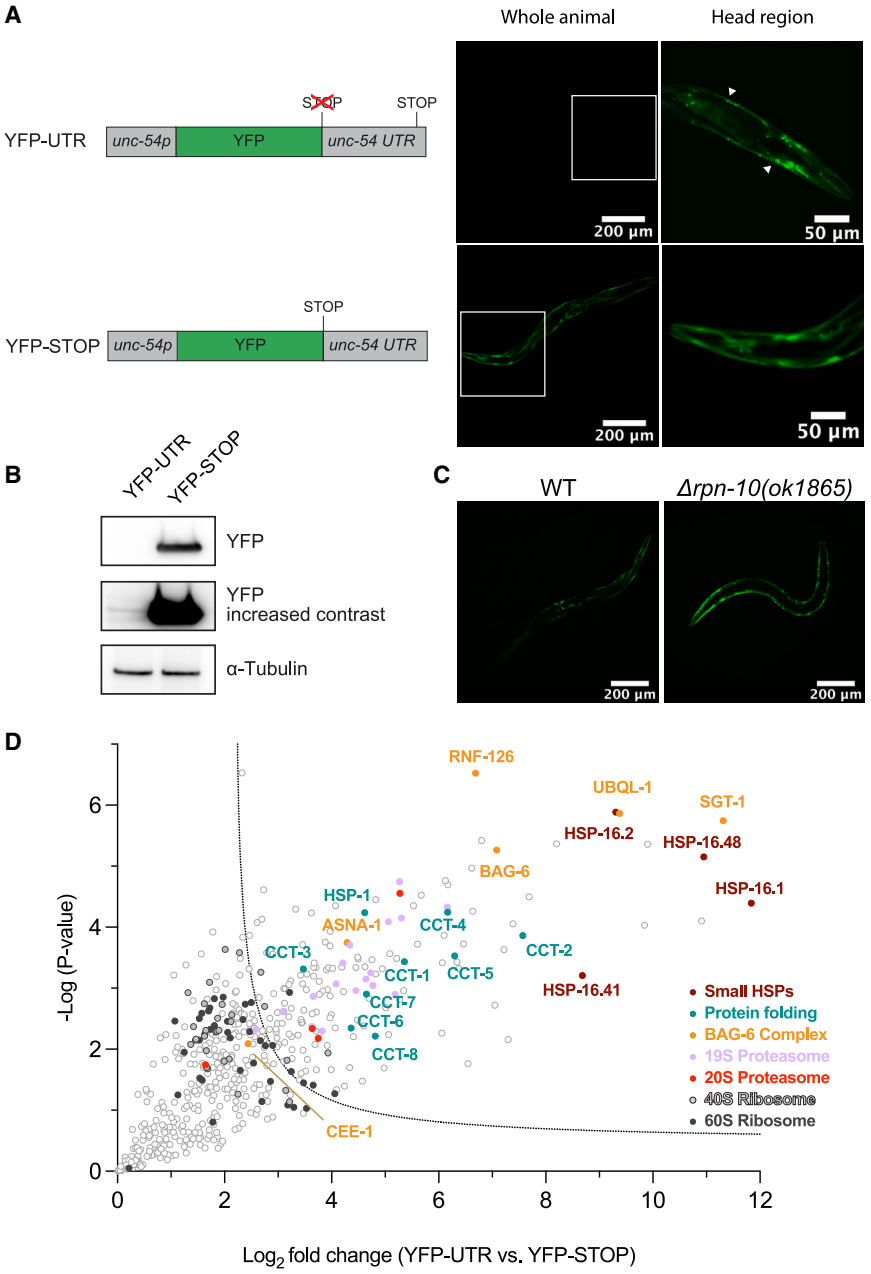

Figure 1. Stop codon readthrough proteins are unstable and recruit specific protein quality control machinery

(A) Expression of readthrough reporter protein in *C. elegans* muscle cells. Left: reporter constructs YFP-UTR, allowing readthrough into the *unc-54* UTR, and YFP-STOP used as control. Right: fluorescence microscopy images of animals expressing these proteins. White boxes indicate head region (magnified and contrast adjusted) (exposure 4ms). Arrow heads point to inclusions of YFP-UTR.

(B) Immunoblot analysis of lysates from adult worms expressing YFP-UTR and YFP-STOP using anti-GFP antibody, revealing the destabilization of YFP-UTR. α-Tubulin served as loading control (n = 3).

(C) Fluorescence microscopy images of wild-type (WT) and Δ*rpn-10* worms expressing YFP-UTR (exposure 100 ms).

(D) Volcano plot representation of label-free proteome analysis of YFP pull-down fractions from worm lysates as in (B). Components of the BAG6 complex, proteasomes, TRiC/CCT chaperonin, and molecular chaperones, including sHSPs and HSP-1, are significantly enriched on YFP-UTR. Selected proteins are annotated. See also Figure S1 and Table S1A.

binding protein GCN1 (general control non-derepressible protein 1) to be critical in recruiting the CCR4/NOT complex for mRNA decay. GCN1 was initially shown to sense uncharged tRNAs at the ribosome A-site upon amino acid starvation, resulting in eIF2α phosphorylation via GCN2 kinase[26] and global downregulation of translation as part of the integrated stress response (ISR).[27] More recently, this function was linked to GCN1 binding to collided ribosomes (disomes) upon translational stalling.[28–30] Using selective ribosome profiling of monosomes and disomes, we show that GCN1 recognizes ribosomes collided at nonoptimal codons in 3′ UTRs, transmembrane proteins, and collagens. GCN1 then recruits CCR4/NOT and other quality control factors, shaping global mRNA turnover. These results position GCN1 as a key translational regulator of proteostasis, a function with increasing importance in adjusting translational dynamics during aging.

RESULTS

BAG6 complex mediates clearance of proteins with translated 3′ UTRs

To study the clearance of readthrough translation products, we generated *C. elegans* strains expressing YFP constructs with and without termination codons (YFP-STOP and YFP-UTR, respectively) in muscle cells. YFP-UTR allows the translation of 115 residues of the *unc-54* 3′ UTR up to a stop codon before the poly(A) site (Figure 1A). Unlike YFP-STOP, YFP-UTR was only weakly detected by fluorescence microscopy and immunoblotting of worm extracts (Figures 1A and 1B). Cells expressing YFP-UTR contained foci consistent with aggregate inclusions (Figure 1A). Depletion of the RPN-10 proteasome subunit increased YFP-UTR levels (Figure 1C), suggesting that YFP-UTR undergoes proteasomal degradation, as previously reported for other readthrough reporter constructs.[16,20,23]

To identify factors that facilitate readthrough protein clearance, we performed pull-down experiments and mass spectrometry to analyze the YFP-UTR interactome, using YFP-STOP as a control. We found the BAG6 chaperone complex, involved in TA

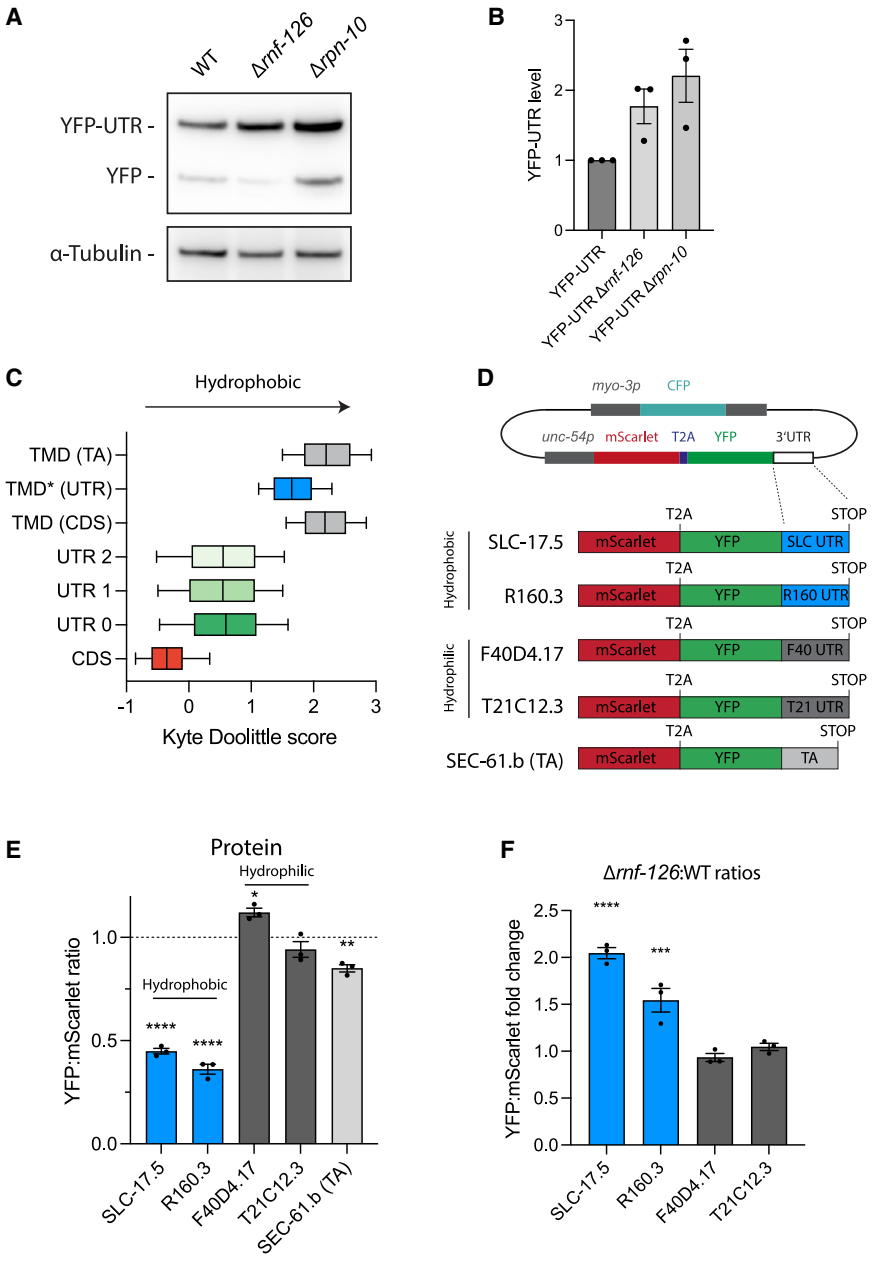

Figure 2. Readthrough reporter proteins with hydrophobic CTEs undergo RNF126-dependent degradation

(A) Immunoblot analysis of wild-type, Δ*rnf-126*, and Δ*rpn-10* worms expressing YFP-UTR using anti-GFP antibody (n = 3). α-Tubulin served as loading control.

(B) Densitometric analysis of immunoblots shown in (A). Error bars represent mean ± SEM (n = 3).

(C) Hydrophobicity (Kyte Doolittle scores [KDSs]) of transmembrane domains of predicted TA-proteins (TMD [TA]; 338 proteins), predicted TMDs in 3′ UTRs (TMD* [UTR] in reading frame 0; 2,323 genes), and predicted TMDs in coding sequences of single-pass membrane proteins (TMD [CDS]; 2,022 proteins) compared with all coding sequences (CDSs) in the *C. elegans* genome (26,584 proteins). TMDs were predicted using Phobius.[38]

(D) Constructs for ratiometric analysis of effects of readthrough into 3′ UTRs encoding hydrophilic F40D4.17 (KDS = −2.29; 36 residues) and T21C12.3 (KDS = −1.91, 34 residues) or hydrophobic SLC-17.5 (KDS = 2.78, 26 residues) and R160.3 (KDS = 2.69, 29 residues) CTE sequences. SEC-61.b was used as an authentic TA-protein, with its tail-anchor region (TA) (29 residues) fused C-terminally to YFP.

(E) Relative destabilization of reporter proteins with hydrophobic CTEs. Ratiometric analysis (YFP:mScarlet ratios) from fluorescence microscopy images of worms expressing constructs described in (D). Experiments were performed in triplicates with at least 5 images per replicate. *p < 0.05; **p < 0.01; ***p < 0.001; ****p < 0.0001 by Dunnett's test. Error bars represent mean ± SEM. Dotted line indicates respective STOP controls.

(F) Selective stabilization of proteins with hydrophobic CTEs in Δ*rnf-126* mutant worms. Fold changes in YFP:mScarlet ratios are indicated. Experiments were performed in triplicates with at least 5 images per replicate. Also see Figure S2. *p < 0.05; **p < 0.01; ***p < 0.001; ****p < 0.0001 by Dunnett's test. Error bars represent mean ± SEM.

membrane protein quality control,[24,31] to be most enriched on YFP-UTR (Figure 1D), comprising BAG-6, the chaperone SGT-1 (SGTA in mammals), the E3 ubiquitin ligase RNF126, as well as UBQL-1, ASNA-1 (GET3 in mammals), and CEE-1 (GET4 in mammals). Additionally, proteasome subunits and molecular chaperones, including small HSPs (HSP-16), the Hsp70 protein HSP-1, and the chaperonin TRiC/CCT, were identified. Ribosomal subunits were borderline enriched, suggesting that both ribosome-associated and completely synthesized YFP-UTR were analyzed. HSP-16 proteins are highly upregulated during stress conditions and aging.[32–35] Indeed, several HSP-16 members were ~30- to 100-fold upregulated upon the expression of YFP-UTR (Figures S1A and S1B), indicating stress response induction. Moreover, HSP-16.1 colocalized with YFP-UTR inclusions, as observed upon the coexpression of YFP-UTR and HSP-16.1-RFP (Figure S1C).

The identification of the BAG6 complex as a major interactor of YFP-UTR suggested that readthrough proteins coopt the quality control machinery of mislocalized TA-proteins. In this pathway, TA-proteins are either handed over from BAG6 to GET4 for membrane integration or, if identified as faulty, ubiquitylated by RNF126 for degradation.[25,36] Accordingly, we found that the deletion of RNF126 stabilized YFP-UTR (Figures 2A, 2B, and S1D). The *unc-54* 3′ UTR is enriched in hydrophobic amino acids (Figure S1E) and apparently functions as a C-terminal degron-like sequence.[37] This trend for hydrophobic residues holds for most *C. elegans* 3′ UTR sequences in all three reading frames.[19] Notably, these sequences are often predicted to contain transmembrane domains (TMDs)[38] similar in hydrophobicity to *bona*

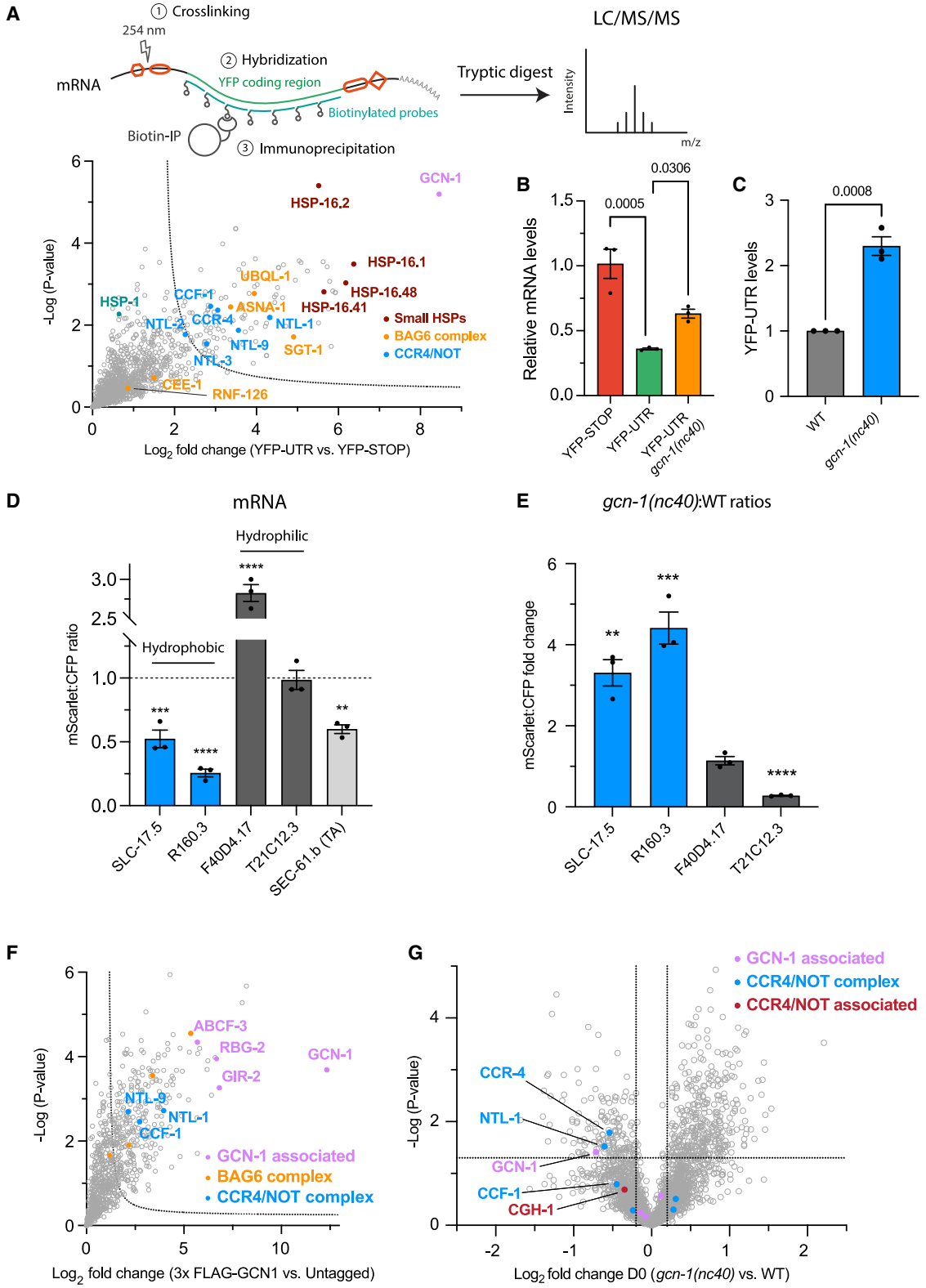

Figure 3. Identification of GCN-1 and CCR4/NOT as quality control factors mitigating stop codon readthrough

(A) Upper: schematic of mRNA pull-down of YFP-UTR and YFP-STOP. Lower: interactome analysis of YFP-UTR mRNA (vs. YFP-STOP). Volcano plots of label-free proteome analysis of pull-down fractions showing enrichment of GCN-1, BAG6 complex, CCR4/NOT, and sHSPs on YFP-UTR. See also Table S1B.

(legend continued on next page)

fide TAs (Figure 2C). Although hydrophobicity is weaker in human 3′ UTRs, the encoded sequences contain similar hydrophobic stretches of ~21 residues (independent of the reading frame), corresponding to the average TA length (Figure S2A). The overall hydrophobicity of *C. elegans* 3′ UTRs arises from their relatively high uracil (U)-content compared with the coding regions of transcripts (Figure S2B), as codons of hydrophobic amino acids, overrepresented in integral membrane proteins, contain ~50% U.[39] Interestingly, higher U-content correlates with a lower tRNA adaptation index (tAI), a proxy for codon optimality (Figure S2C). Most 3′ UTRs contain an in-frame stop codon before the poly(A) site, irrespective of reading frame[19] (Figure S2D).

To investigate whether hydrophobic CTEs are degraded preferentially, we generated tricolor expression constructs encoding CFP and mScarlet-T2A-YFP under individual promoters (Figure 2D). The presence of a self-cleaving T2A site results in the expression of mScarlet and either YFP alone or YFP fused with a hydrophobic or hydrophilic CTE (modeling 3′ UTR readthrough events) as individual proteins from the same mRNA, allowing the assessment of protein stability by YFP:mScarlet ratios. CFP, expressed from a separate mRNA, served as copy-number control. Using ratiometric imaging (see STAR Methods), we compared how two length-matched (26–36 residues) hydrophobic (SLC-17.5 and R160.3) or hydrophilic (F40D4.17 and T21C12.3) 3′ UTR-encoded CTEs affected protein stability (Figure 2D). Hydrophobic CTEs were destabilizing, indicated by low YFP:mScarlet ratios (Figures 2E, S2E, and S2F). A fusion protein containing the C-terminal membrane span of the TA-protein SEC-61.b (mScarlet-T2A-YFP-TA) was mildly destabilized (Figure 2E), consistent with membrane targeting protecting against degradation.[31] Importantly, RNF-126 mutation stabilized hydrophobic CTEs but weakly affected hydrophilic constructs (Figure 2F).

Thus, the BAG6 complex recognizes proteins with hydrophobic CTEs encoded by 3′ UTRs and mediates their degradation, similar to the clearance of TA-proteins that fail membrane insertion.

Readthrough leads to mRNA decay via GCN-1 and CCR4/NOT recruitment

It remains unclear whether mRNA degradation ameliorates CTE protein accumulation generated by 3′ UTR readthrough. Using mRNA sequencing (mRNA-seq), we detected a ~70% reduction in the mRNA levels of YFP-UTR relative to YFP-STOP (Figure S3A). qPCR analysis of mRNA levels, corrected for transgene copy number, confirmed these results (Figures S3B and S3C). To test whether the SKI-exosome complex degrades readthrough mRNAs, as shown for non-stop mRNA,[40–42] we generated SKIH-2 (RNA helicase component) mutant worms expressing YFP-UTR. SKIH-2 deletion did not stabilize readthrough mRNAs, suggesting alternative decay routes (Figure S3C).

To identify factors mediating YFP-UTR mRNA decay, we performed *in vivo* crosslinking and RNA immunoprecipitation, followed by mass spectrometry[43] (Figure 3A; STAR Methods), with YFP-STOP as control. The BAG6 complex and sHSPs were enriched in the YFP-UTR mRNA pull-down (Figure 3A), indicating cotranslational recruitment. We additionally found GCN-1 to be highly enriched, a >2,600 amino acid protein predominantly composed of HEAT domains that binds collided ribosomes.[30] Interestingly, GCN-1 was also enriched in the YFP-UTR protein interactome (Table S1A). In addition, several components of CCR4/NOT, a multi-protein complex combining 3′ to 5′ exonuclease and E3 ligase activities,[44] were identified as interactors of YFP-UTR mRNA (Figure 3A), including the exonucleases CCF-1 and CCR-4.

Although functions of CCR4/NOT in mRNA degradation are well established,[45,46] GCN-1 has not been implicated in mRNA turnover. To explore possible roles of GCN-1 in regulating readthrough mRNA decay, we used the hypomorphic *gcn-1(nc-40)* mutant allele, in which GCN-1 is N-terminally truncated, lacking 244 amino acids required for full function.[47,48] Note that GCN-1 is essential in metazoans and cannot be deleted.[49] Upon expression in *gcn-1(nc40)* mutants, both mRNA and protein levels of YFP-UTR were partially restored (Figures 3B, 3C, and S3D). To explore the effects of GCN-1 dysfunction on the expression of hydrophobic and hydrophilic CTEs, we used tricolor expression constructs introduced above (Figure 2D). Based on mScarlet:CFP ratios, mRNAs encoding hydrophobic CTEs were destabilized in wild-type (WT) animals, whereas transcripts encoding hydrophilic CTEs either remained unchanged compared with STOP controls or were more stable (Figure 3D). Interestingly, mRNAs of the reporter containing the TA sequence of SEC-61.b (SEC-61.b(TA)) were also destabilized, suggesting that without full-length mRNA and protein context, the TA-region triggers mRNA degradation as for readthrough reporters. GCN-1 mutation stabilized mRNAs encoding hydrophobic CTEs 3- to 5-fold (Figure 3E) and either did not affect or destabilized (e.g.,

(B) qPCR analysis of YFP-STOP and YFP-UTR mRNA levels in wild-type *C. elegans* and in *gcn-1(nc40)* mutant animals (n = 3). Data were analyzed using the $2^{(-\Delta\Delta CT)}$ formula, and p values were calculated using Fisher's least significant difference (LSD) test (see STAR Methods). Error bars represent mean ± SEM.

(C) YFP-UTR protein levels in wild-type and *gcn-1(nc40)* mutant worms. Analyses by immunoblotting as in Figure S3D were quantified by densitometry (n = 3). p value calculated from unpaired Student's t test. Error bars represent mean ± SEM.

(D) Ratiometric analysis of mRNA levels (mScarlet:CFP ratios) of the indicated hydrophilic and hydrophobic readthrough constructs (Figure 2D) from fluorescence microscopy images of worms. Experiments were performed in triplicates with at least 5 images per replicate. *p < 0.05; **p < 0.01; ***p < 0.001; ****p < 0.0001 by Dunnett's test. Error bars represent mean ± SEM. Dotted line indicates STOP controls.

(E) Selective stabilization of mRNA levels of hydrophobic readthrough constructs in *gcn-1(nc40)* mutant animals. Fold change in mRNA levels determined as in (D). Experiments were performed in triplicates with at least 5 images per replicate. *p < 0.05; **p < 0.01; ***p < 0.001; ****p < 0.0001 by Dunnett's test. Error bars represent mean ± SEM.

(F) Interactome analysis of GCN-1. Volcano plot representation of label-free proteome analysis of anti-FLAG pull-down from lysates of worms expressing endogenous 3xFLAG-GCN-1 relative to lysates from untagged animals. Selected proteins are annotated. See also Table S1C.

(G) Volcano plot representation of label-free proteome analysis of polysome fractions of young (day 0) *gcn-1(nc40)* mutant worms relative to polysome fractions of day 0 wild-type animals. Selected proteins are annotated. Dotted lines indicate cutoffs for enrichment at the x axis ($\log_2 \pm 0.2$, ~1.15-fold) and at the y axis for p values (0.05, $-\log > 1.33$). See also Figure S3J and Table S1D.

for T21C12.3) hydrophilic CTE mRNAs. Thus, GCN-1 facilitates mRNA decay of readthrough reporters when their 3′ UTRs encode hydrophobic CTEs.

Lacking a known mRNA-destabilizing enzymatic activity, it seemed unlikely that GCN-1 acts directly on readthrough transcripts but rather functions as a platform in recruiting additional factors to ribosomes.[50] To identify such interactors, we tagged endogenous GCN-1 with an N-terminal 3xFLAG, followed by immunoprecipitation and mass spectrometry. The tagged protein associated with polysomes is similar to WT GCN-1[26] (Figure S3E). Besides known GCN-1 interactors, including ABCF-3 (ABCF3), GIR-2 (RWDD1), RBG-2 (DRG2), and MBF1 (EDF1),[30] GCN-1 pull-down enriched multiple components of the CCR4/NOT complex (CCR-4, CCF-1, and NTL-1) and the BAG-6 complex (SGT-1, UBQL-1, CEE-1, and ASNA-1) (Figure 3F). These results prompted us to hypothesize that GCN-1 senses readthrough events and mediates the cotranslational recruitment of CCR4/NOT to initiate mRNA decay. To test this, we analyzed polysome fractions from young adult (day 0) WT and *gcn-1(nc40)* nematodes by mass spectrometry (Figure S3F). Polysomes of mutant worms showed a lower GCN-1 content (Figure 3G). CCR4/NOT and its cofactor CGH-1 (DDX6 in mammals)[51] were proportionally reduced. The ~30% reduction of CCR4/NOT on polysomes could broadly affect mRNA homeostasis, given its function as a major cytosolic deadenylase.[52]

Based on these data, GCN-1 recruits CCR4/NOT facilitating readthrough mRNA decay, while the BAG6 complex mediates the degradation of readthrough proteins.

Conserved mechanisms of mammalian readthrough mitigation

Are the quality control pathways of translational readthrough conserved in mammalian cells? To address this question, we chose the 32 residue 3′ UTR of transcription elongation factor A protein-like 1 (TCEAL1), encoding a hydrophobic CTE, and expressed it as a YFP fusion protein in human HEK293T cells. Interactome analysis by mass spectrometry identified components of the BAG6 and CCR4/NOT complexes, as well as the sHSP HSPB1 and other chaperones (Figures S4A and S4B), reflecting results obtained in *C. elegans*. GCN1 was not significantly enriched, unlike the YFP-UTR interactome in *C. elegans* (Table S1A). To analyze the stability of both protein and corresponding mRNA, we expressed two length-matched fusion proteins translating either hydrophobic CTEs (3′ UTR of TCEAL1 and olfactory receptor 8D4 [OR8D4]) or relatively hydrophilic CTEs (3′ UTR of protein cornichon homolog 3 [CNIH3] and cholecystokinin [CCK]), employing ratiometric reporter constructs (Figure 4A; see legend for Kyte Doolittle scores [KDSs]). Dual CMV promoters drove the expression of mScarlet-2xT2A-YFP fused to the 3′ UTR of interest and mTurquoise2 as copy-number control, allowing simultaneous assessment of protein stability (YFP:mScarlet ratios) and mRNA levels (mScarlet:mTurquoise2 ratios) by flow cytometry (Figures 4A and S4C; see STAR Methods). As in *C. elegans*, hydrophobic CTEs displayed lower stability than hydrophilic CTEs, both at protein and mRNA levels (Figures 4B and 4C). The TA sequence of SEC61B (SEC61B(TA)) was also destabilizing (Figures 4B and 4C).

To investigate readthrough protein degradation mechanisms in mammalian cells, we introduced perturbations to the pathway identified in *C. elegans*. The ubiquitin-activating enzyme (E1) inhibitor MLN-7243 stabilized reporter proteins with hydrophobic CTEs (TCEAL, OR8D4, SEC61B(TA)) (Figure S4D, left). The lysosomal inhibitor bafilomycin A1 only mildly stabilized OR8D4 but had a more significant effect on SEC61B(TA) (Figure S4D, right). Stabilization of TCEAL1 by E1 inhibition induced its sedimentation into the insoluble fraction (Figure S4E) and formation of intracellular inclusions (Figure S4F). In contrast, hydrophilic CTEs remained soluble and diffusely distributed (Figure S4F). Depletion of BAG6 and RNF126, but not SGTA, by CRISPR-Cas9 (Figure S4G) also stabilized reporter proteins with hydrophobic CTEs and the reporter containing the TA sequence of SEC61B (Figure 4D). This effect was more pronounced with the CTE of the TCEAL1 3′ UTR than with the similarly hydrophobic CTE of OR8D4 or with SEC61B(TA), suggestive of redundant chaperone machineries for proteasomal degradation of certain readthrough proteins. Although RNF126 is mainly responsible for degrading mistargeted TA-proteins,[36] the human BAG6 complex associates with a homologous E3 ligase, RNF115.[36] Indeed, combined deletion of RNF126 and RNF115 further stabilized the TCEAL1 fusion construct (Figures 4D, S4H, and S4I). These results suggest that mammalian cells use the BAG6 complex to degrade hydrophobic readthrough products, and failure thereof can result in aggregation.

We next investigated whether CCR4/NOT contributes to readthrough mRNA decay in HEK293T cells. Because several CCR4/NOT complex members are essential, we used siRNA to downregulate (by ~75%) the scaffolding subunit CNOT1 (Figures S4J and S4K). This significantly, albeit modestly, stabilized mRNAs encoding CTE proteins of TCEAL, OR8D4, and SEC61B(TA) (hydrophobic) but not CNIH3 or CCK (hydrophilic) (Figure S4L).

Together, these results show that the two-tiered quality control pathway for readthrough mitigation involving the clearance of protein and mRNA operates in human cells.

Endogenous substrates of GCN-1 surveillance

Recent structural evidence showed that the solenoid HEAT repeats of GCN1 bracket disomes.[30] To identify endogenous mRNA targets of GCN-1-mediated quality control, we performed GCN-1 selective ribosome profiling of monosomes and disomes[29,53–61] in nematodes expressing endogenous 3xFLAG-tagged GCN-1. Profiling of total ribosomes served as input control. Although most ribosome-protected footprints (RPFs) associated with GCN-1 mapped to open reading frames (ORFs), RPFs of GCN-1-bound monosomes were ~4-fold enriched in 3′ UTRs and disomes ~10-fold enriched compared with input (Figures 5A and 5B), providing independent evidence for the role of GCN-1 in readthrough mitigation. Note that disomes were ~2-fold more frequent in 3′ UTRs than monosomes in the input control (Figure 5B, gray bars). Most GCN-1-associated 3′ UTRs contained stop codons upstream of the poly(A) tails, resulting in CTEs of up to 570 amino acids. We noted increased GCN-1 binding within ~10–20 codons after annotated termination codons (Figure 5A, right). These sequences were enriched in codons for hydrophobic amino acids (phenylalanine, leucine, and isoleucine), whereas codons of polar and charged

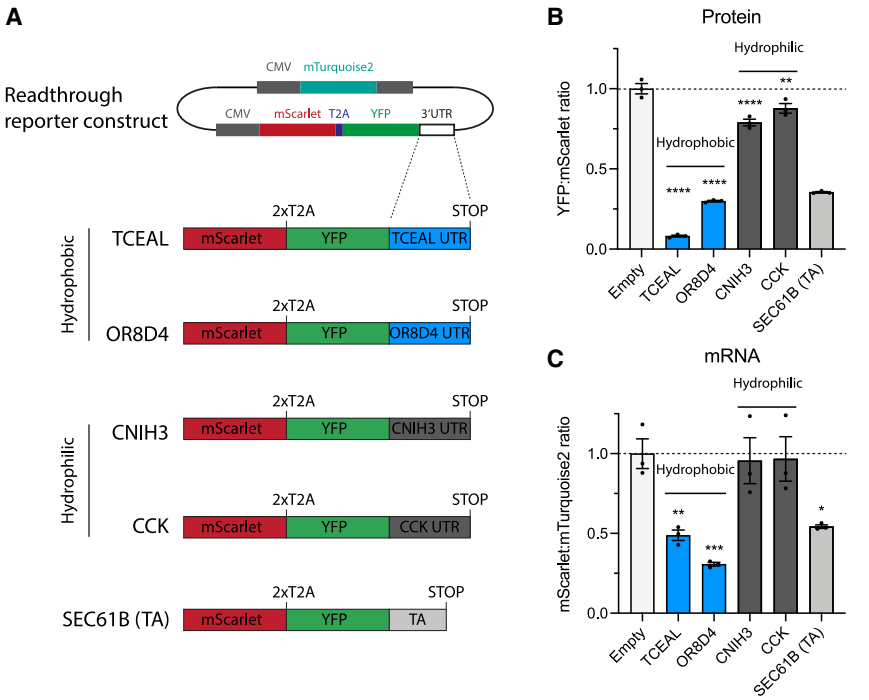

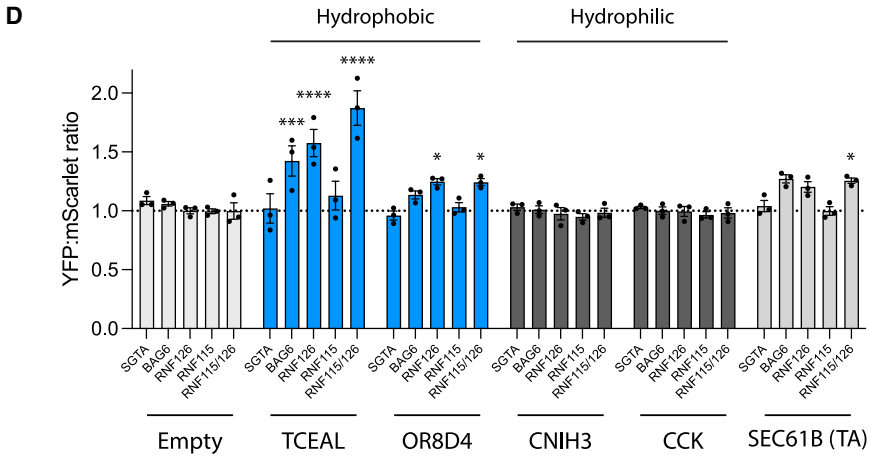

Figure 4. Readthrough mitigation pathways are conserved in mammalian cells

(A) Constructs for ratiometric analysis by flow cytometry of effects of readthrough into 3′ UTRs encoding hydrophobic (transcription elongation factor A protein-like 1 [TCEAL1], KDS = 2.07, 32 residues; olfactory receptor 8D4 [OR8D4], KDS = 1.96, 28 residues) or hydrophilic (protein cornichon homolog 3 [CNIH3], KDS = −2.21, 34 residues; cholecystokinin [CCK], KDS = −1.89, 26 residues) CTE sequences in HEK293T cells. The TA sequence of SEC61B was also analyzed.

(B and C) Ratiometric analysis in HEK293T cells of protein levels (YFP:mScarlet ratio) (B) and of mRNA levels (mScarlet:mTurquoise2 ratio) (C) of constructs in (A). Data from flow cytometry (see Figure S4C). *p < 0.05; **p < 0.01; ***p < 0.001; ****p < 0.0001 by Dunnett's test. Error bars represent mean ± SEM (n = 3). Dotted line indicates empty control ratios.

(D) Effects of the deletion of genes encoding factors involved in readthrough mitigation on protein levels of hydrophilic and hydrophobic readthrough constructs, determined as in (B). Error bars represent mean ± SEM (n = 3). *p < 0.05; **p < 0.01; ***p < 0.001; ****p < 0.0001 by Dunnett's test. Dotted line indicates wild-type ratios.

residues (arginine, threonine, and glutamine) were relatively depleted (Figure S5A; Table S2C), supporting the finding that GCN-1 preferentially mediates quality control of readthrough proteins with hydrophobic CTEs. Furthermore, 3′ UTRs are enriched in nonoptimal codons (low tAI scores) (Figure S5B), a feature correlating with hydrophobicity (see Figure S2B), suggesting that GCN-1 may sense disome formation resulting from slowed translation.

We next analyzed the properties of GCN-1-associated RPFs in coding sequences (CDSs). TMD protein and collagen mRNAs were enriched among GCN-1-bound monosomes and disomes (Figure S5C; Tables S2D and S2E). These transcripts generally showed increased disome frequencies (Figure S5D; Table S2F). In GCN-1-specific disomes translating TMD mRNAs, the leading ribosome was preferentially positioned ~15 nucleotides (~5 amino acids) after a TMD (~25 amino acids) fully emerges from the ribosome exit tunnel,[62] assuming that the tunnel accommodates up to ~40 amino acids[63] (Figure 5C). This TMD has likely engaged the membrane insertion machinery, whereas on the colliding ribosome, the TMD would have only partially emerged (Figure 5C). Interestingly, profiling of total ribosomes (monosomes) from *gcn-1(nc40)* mutants showed decreased ribosome density after TMD emergence compared with WT (Figure 5C). Thus, GCN-1 may sense problematic insertion of complex membrane proteins resulting in translational slowdown and ribosome collisions.[54,64,65] Consequently, GCN-1 surveillance could mediate mRNA decay as for readthrough proteins. Indeed, numerous mRNAs were dysregulated in *gcn-1(nc40)* mutant nematodes (Table S3A), consistent with reduced CCR4/NOT recruitment to polysomes (Figure 3G). Although TMD transcripts were mildly stabilized in young (day 0) *gcn-1(nc40)* mutant animals, mRNAs of TMD proteins targeted by GCN-1 (4 or more membrane spans; Table S3C) were significantly stabilized in aged (day 6) *gcn-1(nc40)* nematodes (Figure S5E; Table S3C). As for 3′ UTRs, TMD transcripts are generally biased toward nonoptimal codons, which was pronounced in TMD transcripts susceptible to GCN-1-mediated mRNA decay (Figure S5F; Table S3C). GCN-1 thus regulates the translation dynamics of TMD proteins and adjusts levels of TMD-encoding mRNAs in an age-dependent manner.

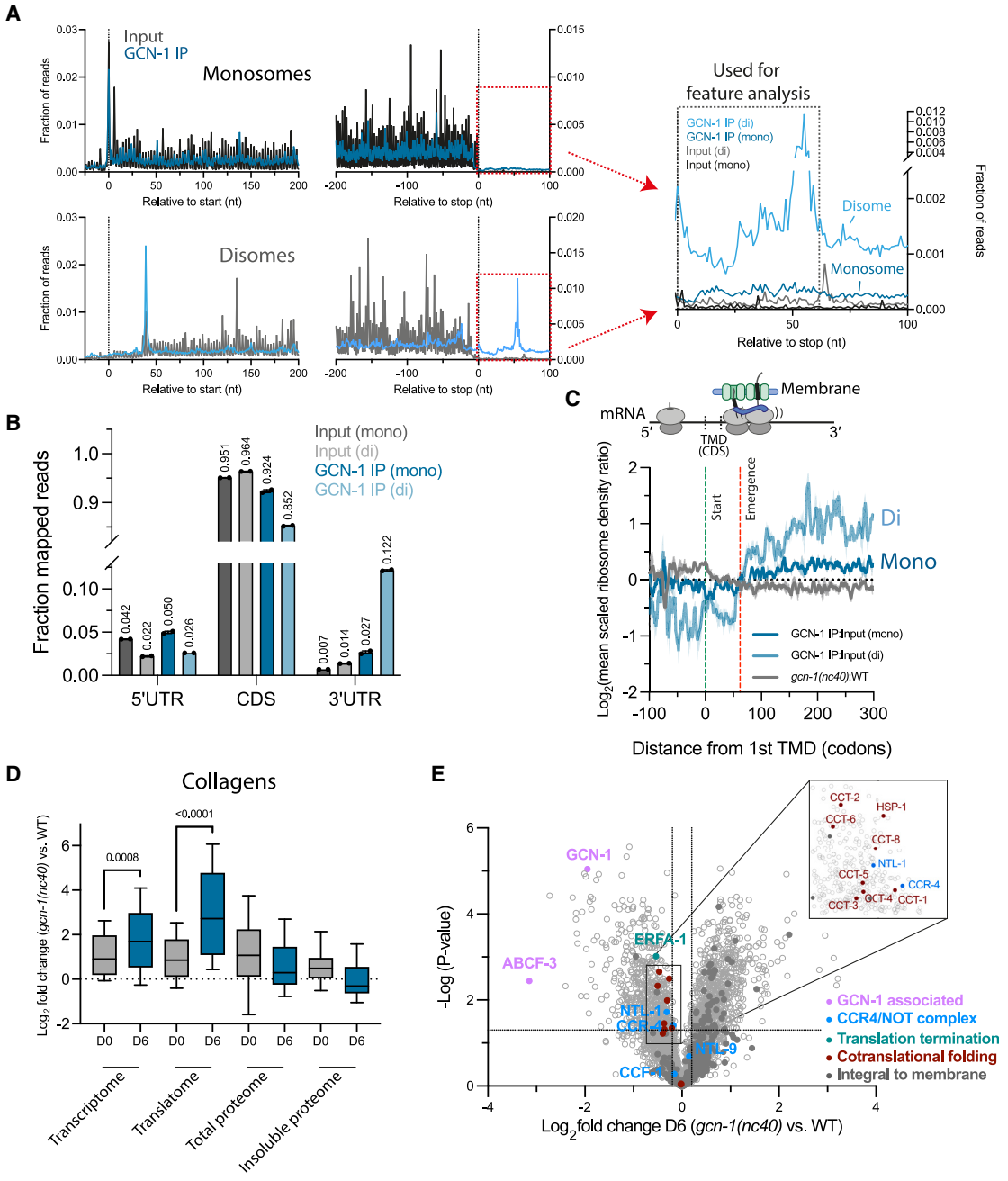

Figure 5. Selective ribosome profiling reveals GCN-1 binding to hydrophobic ribosomes translating 3′ UTRs, TMD proteins, and collagens

(A) Metagene plots of GCN-1-bound ribosomes (monosomes and disomes) and total input control are shown (3′ UTR regions magnified in right) (see STAR Methods).

(B) Distribution of RPFs of GCN-1-IPed ribosomes and total input control in 5′ UTR, coding sequences (CDSs) and 3′ UTR regions of monosomes and disomes. Mean values are indicated above bars.

(C) Metagene analysis of GCN-1 interaction with TMD protein transcripts. RPFs of GCN-1 bound monosomes (odds ratio compared with total input; n = 1,303; blue line ± SEM in light blue), disomes (n = 2,595; light blue line ± SEM shaded) and ribosomes of *gcn-1(nc40)* mutant animals (odds ratio compared with wild type; n = 1,029; dark gray line ± SEM in light gray) are shown. Each transcript was centered around the onset of the first TMD (position 0, green dotted line) and RPFs were expressed as mean-scaled ribosome densities (normalization window of 300 codons up- and downstream of TMD start, position 0). Full emergence of TMDs from the ribosome exit tunnel is indicated by the red dotted line at codon position 65, assuming an average TMD length of 25 codons and a ribosomal exit tunnel length of 40 codons.

(D) Age-dependent effects of GCN-1 dysfunction on the transcriptome (n = 130), translatome (n = 110), total proteome (n = 39), and insoluble proteome (n = 29) of collagens. Young (day 0) and old (day 6) *gcn-1(nc40)* mutant worms were analyzed relative to young (day 0) and old (day 6) wild-type nematodes, respectively. The

(legend continued on next page)

To test whether GCN-1 dysfunction causes TMD protein misfolding and aggregation, we analyzed detergent-insoluble fractions of *gcn-1(nc40)* mutant and WT animals using mass spectrometry. Consistent with the age-dependent effects of GCN-1 observed above, TMD proteins were significantly insoluble in day 6 *gcn-1(nc40)* animals (Figure S5G; Table S1H), resulting in upregulation of several unfolded protein response (UPR)-related genes (Table S3B), suggesting that GCN-1 surveillance becomes critical as translational homeostasis undergoes age-dependent decline.[5,35]

Collagen transcripts were also enriched among GCN-1-bound monosome and disome RFPs (Figure S5C; Tables S2D and S2E). Collagens are the main structural component of connective tissue and extracellular matrix.[66,67] Collagen homeostasis is critical for *C. elegans* longevity.[68,69] In line with the role of GCN-1 in regulating collagen biosynthesis, mRNAs of collagen proteins were stabilized in *gcn-1(nc40)* nematodes, an effect enhanced in aged animals (Figure 5D; Tables S3A and S3B). Collagens contain structurally critical X-Pro-Pro (XPP) motifs[70] that induce ribosomal stalling during translation.[71–73] We therefore investigated the effects of GCN-1 on ribosome pausing at tripeptide motifs by computing pause scores based on ribosome occupancies (STAR Methods).[74] Interestingly, pausing at XPP motifs was enhanced in WT animals compared with *gcn-1(nc40)* mutants, which was magnified during aging (Figure S5H), resulting in higher ribosome densities at polyproline stretches in day 6 WT nematodes (Figure S5I). Note that in *gcn-1(nc40)* mutants, ribosome pausing at polyproline motifs, although reduced, remains detectable (Figure S5I). Thus, fully functional GCN-1 appears to increase ribosome residence time at proline-rich motifs. More generally, nonoptimal codons (low tAI scores) increased the recruitment of GCN-1 to monosomes and disomes (Figure S5J), and aged WT animals preserved high ribosome A-site occupancy with nonoptimal codons compared with *gcn-1(nc40)* mutant nematodes (Figure S5K). Collectively, the association of GCN-1 with ribosomes at nonoptimal codons stabilizes disomes, which appears to further reduce elongation speed.

To explore the possible consequences of reduced translational pausing caused by impaired GCN-1 function, we investigated the fate of collagen mRNAs and proteins in young (day 0) and aged (day 6) animals. Stabilization of collagen mRNAs in day 6 *gcn-1(nc40)* worms (Figure 5D; Table S3B) increased collagen protein translation, as indicated by ribosome profiling (Figure 5D; Tables S2A and S2B). However, total collagen protein levels did not increase and rather declined (Figure 5D; Tables S1E and S1F). This mismatch between changes in protein and translation levels in whole animals suggests that *C. elegans* may recognize excess collagen translation products as aberrant and degrade them. Notably, polysome fractions of aged *gcn-1(nc40)* mutant animals contained ~20% reduced amounts of Hsp70 (HSP-1) and TRiC/CCT chaperones (Figure 5E), without changing total abundance (Tables S1E and S1I). This is consistent with the notion that translational slowdown on nonoptimal codons serves in chaperone recruitment.[61] In addition to CCR4/NOT, translation release factor 1 (ERFA-1; eRF1 in mammals) was also reduced in polysomes of aged *gcn-1(nc40)* nematodes (Figure 5E). eRF1 has been shown to mediate premature translation termination on nonoptimal codons.[75]

Together, these findings suggest that GCN-1 functions broadly in translational regulation. By stabilizing colliding ribosomes at nonoptimal codons (enriched in 3′ UTRs, TMD proteins, and collagens), GCN-1 recruits quality control machineries to ensure efficient protein biogenesis and/or mediate mRNA decay. This function is increasingly important during aging.

GCN-1 function is conserved in mammalian cells and is required for stress signaling

To analyze GCN1's role in translational surveillance in mammalian cells, we performed selective ribosome profiling in HEK293T cells. We induced readthrough with a low dose of the aminoglycoside antibiotic G418 in combination with CC-885, a small molecule mediating degradation of the release factor eRF3 (Figure S6A), thereby limiting translation termination capacity.[76,77] GCN1-binding to ribosomes translating into 3′ UTRs was clearly detectable in untreated cells and increased upon treatment with G418 and CC-885 (Figures 6A and 6B). Protein classes targeted by GCN1 within CDSs in untreated cells were essentially identical to those in *C. elegans*, including TMD transcripts and collagens (Figure S6B; Table S2G), despite low expression of the latter in HEK293T.[78]

Mass spectrometry of polysome fractions under enhanced readthrough conditions (Figure S6C) revealed the association of RQC-related factors, including DRG1, promoting translation through stalling-inducing motifs,[79] the translational repressor GIGYF2, and the SKI-exosome component SKIV2L (Figure 6C). Recruitment of these factors is presumably due to readthrough into poly(A) tails. Other RQC-related factors, including the collision sensor, ZNF598, and EIF4E2, were not enriched upon enhanced readthrough (Figure 6C; Table S1J). Besides RQC-related factors, we confirmed the recruitment of GCN1 and the BAG6 machinery, along with the depletion of eRF3 induced by CC-885 (Figure 6C). EDF1 and ZAKα (MAP3K), cooperating with GCN1 in ribosome collision sensing,[29,30,80,81] were also significantly enriched (Figure 6C; Table S1J). ZAKα signals the ribotoxic stress response (RSR) upon ribosome stalling.[29,82]

Stop codon readthrough induced by G418 activates the ISR limiting global translation.[83] We therefore tested whether readthrough sensing by GCN1 is critical for this signaling effect. Note that HEK293T cells tolerate the deletion of GCN1 (Figure S6D). Upon treatment with G418 and CC-885, WT cells showed a time-dependent accumulation of phosphorylated eIF2α (P-eIF2α) and p38 (P-p38) (Figures 6D, S6E, and S6F), indicating ISR and RSR activation.[29] GCN1 deletion suppressed eIF2α phosphorylation and P-p38 was reduced (Figures 6D

horizontal line within boxplots indicates the median; boxes indicate upper and lower quartile and whisker caps 10^{th}–90^{th} percentile, respectively. p values by Holm-Sidak test. See also Tables S1E–S1H, S2A, S2B, S3A, and S3B.

(E) Volcano plot representation of label-free proteome analysis of polysome fractions of old (day 6) *gcn-1(nc40)* mutant worms relative to polysome fractions of day 6 wild-type animals (as in Figure 3G). Selected proteins are annotated. Dotted lines indicate cutoffs for enrichment at the x axis ($\log_2 \pm 0.2$, ~1.15-fold) and at the y axis for p values (0.05, $-\log > 1.33$). See also Figure S3F and Table S1I.

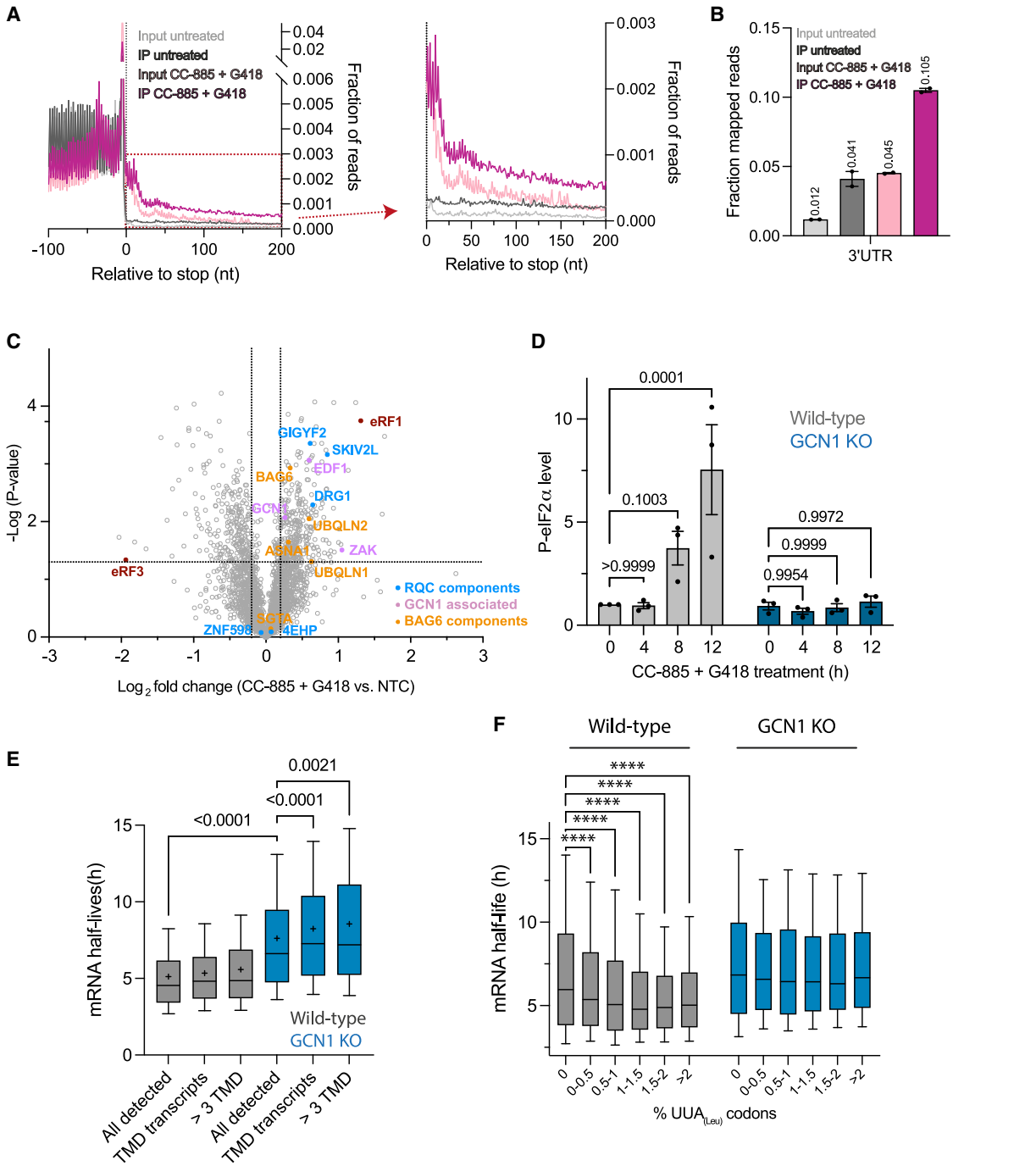

Figure 6. GCN1 function is conserved and critical for stress signaling and mRNA turnover in human cells

(A) Metagene plots of GCN1-selective ribosome profiling data from HEK293T cells upon pharmacologically induced readthrough. GCN1-IPed ribosomes (monosomes) and total input control are shown. When indicated, cells were treated for 4 h with G418 (20 μg/mL) and CC-885 (10 nM).

(B) Distribution of RPFs of GCN1-IPed ribosomes and total input control in 3′ UTR regions in treated (CC-885 + G418; purple) and untreated cells (gray). Mean values are indicated above bars.

(C) Volcano plot representation of label-free proteome analysis of polysome fractions from HEK293T cells treated with G418 and CC-885 as in (A) to induce readthrough relative to polysome fractions of untreated cells. Dotted lines indicate cutoffs for enrichment at the y axis ($\log_2 \pm 0.2$, ~1.15-fold) and at the y axis for p values (0.05, $-\log > 1.33$). See also Figure S6B and Table S1J.

(D) Integrated stress response activation upon induced readthrough. Wild-type and GCN1-deleted HEK293T cells were treated with CC-885/G418 as in (A) for the times indicated. Phospho (P)-eIF2α and P-p38 were detected by immunoblotting of cell lysates and quantified by densitometry. Error bars represent mean ± SEM (n = 3). p values by Holm-Sidak test.

(legend continued on next page)

and S6E). Therefore, GCN1-mediated translational surveillance is conserved in mammalian cells and required for stress signaling upon enhanced readthrough.

GCN1 functions broadly in regulating mRNA turnover

CCR4/NOT regulates cotranslational mRNA turnover by monitoring codon optimality.[52] The ~30% depletion of CCR4/NOT complex from polysomes when GCN1 is dysfunctional (Figures 3G and 5E) would generally affect mRNA deadenylation rates, consistent with numerous transcripts being stabilized in *gcn-1(nc40)* mutant *C. elegans*, including TMD proteins and collagens (Tables S3A and S3B). The ability to delete GCN1 in HEK293T cells allowed us to test this prediction. Sucrose cushion fractionation and immunoblotting confirmed our results from *C. elegans* that HSP70 (HSPA8), TRiC (CCT4), and eRF1 (ETF1) were depleted by ~30% from ribosomes of GCN1 knockout cells (Figure S6H). CNOT3, the CCR4/NOT subunit recognizing slow-decoding ribosomes,[46] was reduced by ~25% on ribosomes (Figure S6H). We measured mRNA decay kinetics using SLAM-seq (thiol(SH)-linked alkylation for the metabolic sequencing of RNA) (Figure S6G; see STAR Methods).[84] We obtained decay curves for ~5,500 transcripts (4 time points) matched for WT and GCN1 deleted cells. Loss of GCN1 profoundly impacted mRNA turnover, increasing the mean mRNA half-life from 5.1 h (WT) to 7.6 h (Figure 6E; Table S4A). Consistent with the binding preferences of GCN1 (Figure S6B), TMD-encoding transcripts were stabilized, increasing their mean half-life from 5.4 to 8.2 h (n = 698) and from 5.6 to 8.6 h for mRNAs encoding proteins with multiple TMDs (n = 168) (Figures 6E, S6I, and S6J). Thus, effects on TMD transcripts contribute to the overall prolonged mRNA half-lives in this dataset. Note that only three collagens (COL7A1, COL12A1, and COL11A2) were reliably detected and showed increased or unchanged half-lives (Table S4A). We attribute this problem to low expression levels of collagens in HEK293T cells.[78]

Codon optimality correlates with mRNA stability, with nonoptimal codons promoting mRNA decay.[85,86] As GCN1 senses codon non-optimality, we next examined the codon dependence of mRNA turnover rates. We calculated codon stability coefficients (CSCs; see STAR Methods) as a measure of how codon-frequencies influence mRNA stability.[85–87] Destabilizing effects of $UUA_{(Leu)}$ codons (tAI = 0.14)[86,87] are shown as a representative example. Although increasing UUA content correlated with shorter mRNA half-lives in WT cells, this effect was diminished upon GCN1 deletion (Figure 6F; Tables S4B and S4C). Generally, mRNA stability was increasingly uncoupled from codon optimality upon GCN1 deletion (Figure S6K; Table S5).

Taken together, GCN1 broadly regulates mRNA stability by monitoring ribosome elongation rates on nonoptimal codons and cooperating with the CCR4/NOT complex to initiate mRNA degradation.

DISCUSSION

Our analysis in nematodes and mammalian cells revealed a two-tiered quality control pathway for clearing both readthrough proteins and mRNAs (Figure 7A). We found that readthrough proteins with hydrophobic CTEs are recognized and targeted for proteasomal degradation by the BAG6 complex, implicated in the quality control of TA membrane proteins. mRNA decay is initiated cotranslationally by the ribosome collision sensor GCN1 and the CCR4/NOT deadenylase complex. Selective ribosome profiling revealed a general function of GCN1 in translational surveillance, with GCN1 preferentially recognizing ribosome slowdown and collision at nonoptimal codons in hydrophobic 3′ UTRs, transmembrane proteins, and collagens (Figures 7A and 7B), thus defining GCN1 as a key regulator of translational dynamics, a function increasingly important during aging.

Readthrough mitigation by quality control machinery of TA-proteins

A key finding is that readthrough protein mitigation in both nematodes and mammalian cells utilizes the BAG6 complex, including SGTA, BAG6, ASNA1 (GET3), GET4, UBL4A, and the E3 ligase RNF126[89] (Figure 7A). BAG6 acts downstream of the cytosolic chaperone SGTA as part of the TA pretargeting module. The pretargeting complex is recruited to ribosomes, poised to capture hydrophobic TA sequences as they emerge from the ribosome exit tunnel.[88,90,91] BAG6 performs a critical triage decision: either transferring the TA client to membrane insertion factors (via GET3 and GET4) or, if unsuccessful, recruiting RNF126 for ubiquitylation and subsequent degradation of TA-proteins.[25,36] We found that the depletion of BAG6 or RNF126 stabilizes readthrough proteins with hydrophobic CTEs, suggesting that such sequences, resembling orphaned TA sequences, are captured by SGTA, followed by transfer to BAG6 and RNF126-dependent proteasomal clearance (Figures 1D, 2B, 2F, and 4D). Lysosomal degradation[21] may be a compensatory pathway when the UPS is inhibited or overtaxed. Bioinformatic analysis showed that CTE sequences of readthrough proteins frequently contain regions with similar characteristics of TA membrane spans (Figures 2C and S2A), potentially causing mislocalization to membranes or aggregation. Consistently, hydrophobic CTE proteins formed aggregate inclusions upon impairing ubiquitylation or proteasome inhibition. Readthrough proteins escaping degradation associated with members of sHSPs, which were upregulated upon overexpression of readthrough constructs (Figures S1A and S1B). sHSPs, in addition to preventing protein aggregation, function in spatial protein

(E) mRNA half-life analysis using SLAM-seq in wild-type and GCN1-deleted cells (n = 5,455), all TMD-encoding transcripts (n = 698) and TMD-encoding transcripts with >3 TMD segments (n =168). The horizontal line within boxplots indicates the median; (+) the mean; boxes indicate upper and lower quartile and whisker caps 10^{th}–90^{th} percentile, respectively. p values were calculated by Holm-Sidak test.

(F) Effect of GCN1 deletion on codon-dependent mRNA decay. Relationship between frequency of $UUA_{(Leu)}$ codons on mRNA half-life. All mRNAs satisfying the goodness of fit (nonlinear regression) criterion of $R^2 > 0.6$ for decay curves (based on T > C conversion rates) were included in the analysis (wild type: n = 8,571; GCN1 knockout [KO]: n = 5,896). The horizontal line within boxplots indicates the median; boxes indicate upper and lower quartile and whisker caps 10^{th}–90^{th} percentile, respectively. ****p < 0.0001 calculated by Holm-Sidak test.

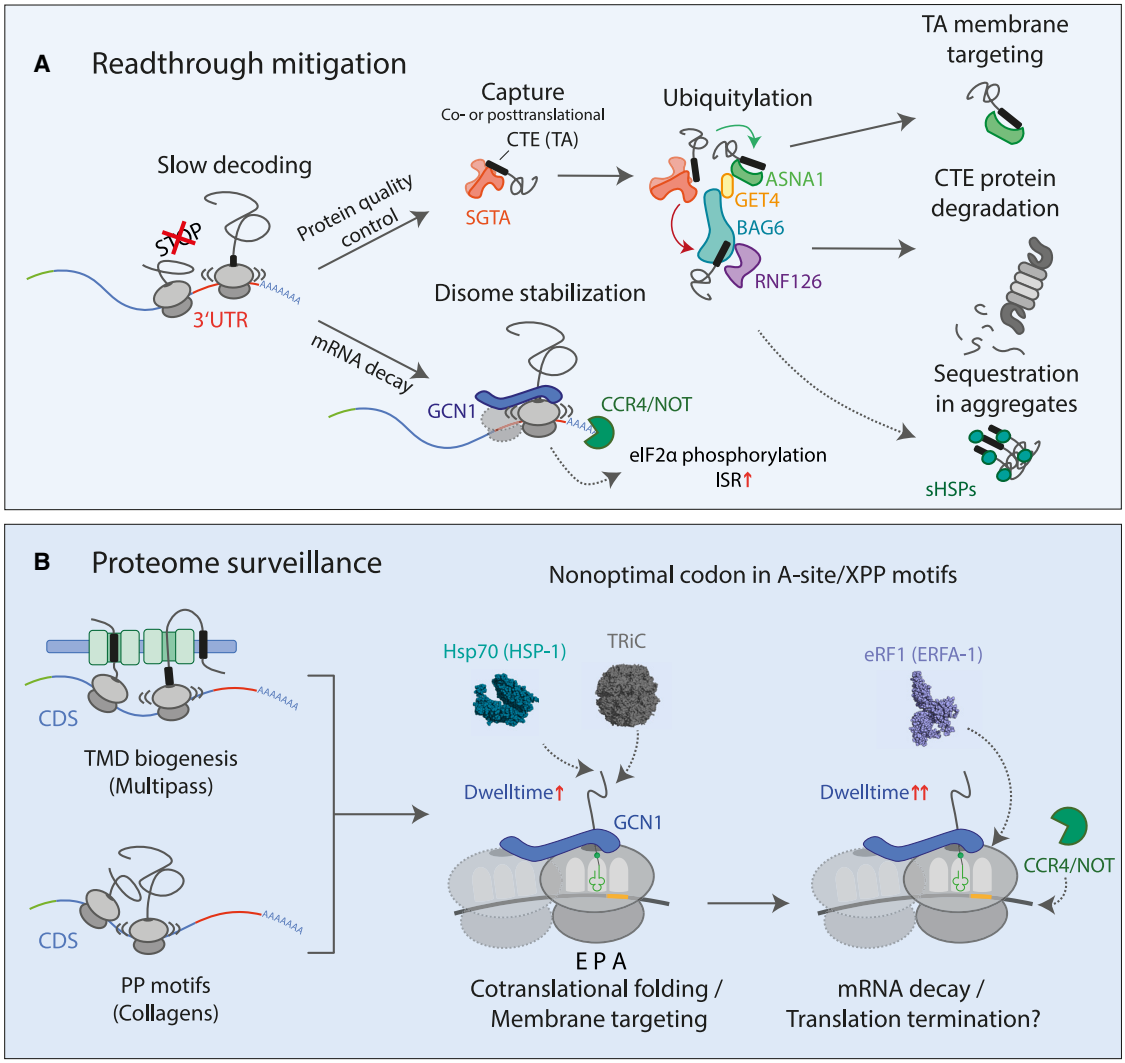

Figure 7. Working model of BAG6 complex and GCN1-CCR4/NOT in readthrough mitigation and proteome surveillance

(A) Model of readthrough mitigation. Readthrough proteins with hydrophobic CTEs resemble TA-proteins and are recognized (co- or posttransationally) by SGTA, which may be recruited to ribosomes before hydrophobic CTEs emerge.[88] Normal TA-proteins are transferred to the membrane targeting module comprising GET4 and ASNA1 (GET3), while, aberrant CTE proteins are captured by the BAG6 complex for RNF126-mediated ubiquitylation and proteasomal degradation. CTE proteins escaping BAG6 surveillance are sequestered by sHSPs into inclusions. Ribosomes translating into hydrophobic 3′ UTRs slow at nonoptimal codons. Colliding ribosomes are recognized by GCN1, which recruits CCR4/NOT to initiate mRNA decay.

(B) Model of general translational surveillance by GCN1. Nonoptimal codons, enriched in TMD protein and collagen transcripts, cause ribosome slowdown and (transient) collisions. GCN1 engages these ribosomes and stabilizes disomes, thereby increasing time available for membrane protein assembly and/or association of chaperones for cotranslational folding. Prolonged ribosome (disome) dwell times, due to biogenesis problems that remain unresolved, may recruit CCR4/NOT to initiate mRNA degradation, thereby limiting aberrant protein production. Recruitment of release factor eRF1 may induce premature chain termination.

quality control by sequestering potentially harmful proteins into aggregates.[92,93] Their upregulation during aging[33,35] is associated with longevity in *C. elegans*. sHSPs may function in parallel to the BAG6 pathway in preventing readthrough proteins to form aberrant protein-protein interactions.

GCN-1-mediated mRNA decay

The readthrough mitigation mechanism revealed an additional layer of quality control wherein translation into a 3′ UTR coding for hydrophobic CTEs, thus enriched in nonoptimal codons (Figures S2A, S2B, and S5B), results in mRNA degradation (Figure 7A). Using mRNA crosslinking and mass spectrometry, we identified the ribosome collision sensor protein GCN1 and the CCR4/NOT deadenylase complex as critical factors in this pathway (Figure 3A). Although functions of CCR4/NOT in mRNA decay are well established,[45,46] GCN1, cofactor of the ISR kinase GCN2,[26,28,29,48] has no known role in mRNA decay. GCN1 dysfunction in nematodes stabilized mRNAs encoding

hydrophobic readthrough reporter proteins (Figure 3E). We found that GCN1 interacts, directly or indirectly, with CCR4/NOT, mediating cotranslational CCR4/NOT complex recruitment for mRNA degradation (Figures 3F and 3G). This function, alongside proteasomal degradation via the BAG6 pathway, limits potentially harmful readthrough protein production.

Considering that readthrough frequencies can reach up to 15% (depending on stop codon sequence context)[10] and most CTEs encoded by 3′ UTRs are hydrophobic, production of readthrough proteins may saturate the quality control capacity of the BAG6 complex for biogenesis of *bona fide* TA-proteins thereby disturbing proteostasis. Recently, the BAG6 complex was implicated in clearing hydrophobic translation products originating from noncoding RNAs other than stop codon readthrough,[94] raising the question of how a single quality control module might deal with such a massive overload. Although redundant protein quality control pathways may operate, we suggest that the mechanism of cotranslational mRNA decay by GCN1 and CCR4/NOT will likely mitigate noncoding RNA translation. By limiting aberrant hydrophobic protein production at the level of translation, the GCN1-CCR4/NOT axis may relieve some of the burdens on the BAG6 complex.

GCN1 function in translational surveillance

GCN1-selective ribosome profiling in *C. elegans* and HEK293T cells uncovered a pervasive function of GCN1 in modulating translation dynamics and proteome balance by regulating mRNA turnover. Apart from 3′ UTRs, we identified numerous CDSs as GCN1 targets, particularly TMD and collagen mRNAs (Figure 7B). As a common denominator, GCN1 interacts preferentially with ribosomes engaged at nonoptimal codons, which frequently occur in these transcripts. Nonoptimal codons result in slow decoding and may induce transient ribosome collisions.[95] Slow-decoding ribosomes are targeted by the CCR4/NOT deadenylase,[46] explaining the codon dependence of mRNA turnover, but whether this depends on ribosome collisions was questioned.[96] Our results indicate that disomes indeed form on nonoptimal codon stretches and are bound by GCN1. This role of GCN1 is consistent with recent evidence that disome formation is widespread across eukaryotic lineages[53,54] and serves to recruit molecular chaperones to address folding of problematic proteins.[54] We suggest that recognition by GCN1 stabilizes such disomes, slowing elongation further (Figures 5C, S5H, S5I, and S5K) to facilitate chaperone recruitment to ribosomes (Figures 5E and S6H). mRNA decay may consequently be initiated by CCR4/NOT (Figure 3G) when folding/biogenesis problems cannot be resolved (Figure 7B). In such situations, translation might be terminated by eRF1 recruitment (Figure 5E), which can execute premature termination on rare codons.[75]

In the case of TMD proteins, translational slowdown is thought to facilitate cotranslational targeting and membrane insertion.[97,98] We found that GCN1 is preferentially recruited to TMD proteins with multiple membrane spans (Figure S5E; Table S3C). Assembly of such proteins is a complex and often inefficient process requiring various membrane insertases, including the Sec61 translocon and the EMC and PAT complexes.[64,99–104] Ribosome profiling revealed that GCN1 tends to engage TMD proteins soon after a transmembrane sequence has emerged from the ribosome (Figure 5C), possibly extending the time available for successful insertion and assembly into membranes. Adapting mRNA levels via CCR4/NOT would limit the risks of overloading chaperone and assembly machineries. Slow decoding also underlies the preferential GCN1 targeting to collagen transcripts. Collagens, the most abundant proteins in mammals, are rich in XPP motifs, with prolines having a critical structural role.[105,106] Prolines slow translation substantially by adopting an unfavorable topology for the peptidyl transferase reaction.[71,72,107,108]

The role of GCN1 in mRNA decay extends beyond collagens and TMD proteins, affecting mRNA stability globally in a codon-dependent manner (Figures 6E, 6F, and S6I–S6K). Given the ~17-fold higher abundance of GCN1 compared with CCR4/NOT,[109] it seems plausible that GCN1 acts upstream of CCR4/NOT. Recent findings that GCN1 engages E3 ligases for ubiquitylation of stalled translation factors[50] support its function as a versatile recruitment platform in translational regulation.

Role of GCN1 in stress signaling and aging

GCN1 is a positive regulator of the ISR induced by amino acid starvation.[26,48] In this signaling pathway, GCN1 activates the GCN2 kinase, which in turn phosphorylates eIF2α, downregulating global translation. Activation of the ISR also occurs upon increased translational readthrough.[83] We found this response is fully dependent on GCN1 (Figure 6D), ruling out secondary effects on eIF2α phosphorylation. Thus, enhanced readthrough is a direct cause of stress activation sensed by GCN1 at ribosomes.

As translational errors are associated with aging,[5,11,110–112] it seemed likely that the wide-ranging role of GCN1 in translational surveillance described here is increasingly relevant during aging. The age-dependent insolubility of TMD proteins upon GCN1 dysfunction is direct evidence of the importance of GCN1 in maintaining RNA and protein balance (Figure S5G). Furthermore, GCN1 dysfunction resulted in an age-dependent increase in mRNA levels and translation for multiple collagens (Figure 5D). However, this was not reflected in higher collagen abundance (Figure 5D). Thus, surplus collagen molecules may be recognized as structurally aberrant, possibly posing a burden on clearance pathways.[113] Indeed, declining collagen integrity is an important aging factor.[105] The profound impact of GCN1 on collagen biogenesis in *C. elegans* illustrates the significance of GCN1-mediated translational surveillance in maintaining proteome balance.

Limitations of the study

We demonstrated that GCN1 functions broadly in translational surveillance maintaining mRNA and protein homeostasis. These findings raise multiple questions: How GCN1 mediates recruitment of CCR4/NOT to slow-decoding ribosomes? Experiments in *S. cerevisiae* showed that CCR4/NOT associates with the ribosome via the NOT5 subunit,[46] suggesting that GCN1 may stabilize NOT5 for ribosome binding. Another open question concerns the exact mechanism by which GCN1 recognizes slow-decoding ribosomes. Does GCN1 bind transiently colliding ribosomes and then stabilize disomes, as the structure of the disome-GCN1 complex suggests,[30] or does it recognize slow-moving

monosomes, reducing elongation speed further to promote disome formation? Finally, it remains to be explored in detail how ribosome engagement by GCN1 facilitates cotranslational folding and membrane protein assembly. It is important to investigate how the loss of translational regulation by GCN1 affects the folding/assembly and turnover of specific proteins, including medically relevant TMD proteins and collagens.

STAR★METHODS

Detailed methods are provided in the online version of this paper and include the following:

- KEY RESOURCES TABLE
- RESOURCE AVAILABILITY
  - Lead contact
  - Materials availability
  - Data and code availability
- EXPERIMENTAL MODEL AND SUBJECT DETAILS
  - *C. elegans* strains and growth conditions
  - Cell culture and transfection
- METHOD DETAILS
  - Cas9 expression and purification
  - CRISPR/Cas9-mediated homologous recombination
  - Immunoblotting
  - LC-MS/MS analysis
  - MS data analysis
  - mRNA pulldown
  - CRISPR knockout cell lines
  - siRNA treatment
  - Flow cytometry
  - Aggregate fractionation
  - Protein pulldown
  - Preparation of total protein extracts for immunoblot analysis
  - Total RNA isolation
  - Quantitative real-time PCR
  - mRNA sequencing
  - Preparation of total ribosome fraction for ribosome profiling
  - Preparation of ribosome fractions for GCN-1 selective ribosome profiling
  - SLAM-seq
  - Polysome gradient analysis
  - SDS-PAGE
  - Microscopy
  - Image analysis
  - Analysis of ribosome profiling and mRNA-seq data
- QUANTIFICATION AND STATISTICAL ANALYSIS

SUPPLEMENTAL INFORMATION

Supplemental information can be found online at https://doi.org/10.1016/j.cell.2023.05.035.

ACKNOWLEDGMENTS

We thank Joshua Arribere and Andrew Fire for providing the *skih-2* mutant *C. elegans* strain. The staff of the MPIB core facility is gratefully acknowledged for technical support with mass spectrometry and next generation sequencing (NGS). Giovanni Cardone from the MPIB imaging core facility is acknowledged for help with image analysis and Assa Yeroslaviz for expert advice on NGS data analysis. We thank Roman Koerner and Liang Zhao for technical support with MS experiments, and Cole Sitron for critically reading the manuscript. Some strains were provided by the Caenorhabditis Genetics Center (CGC), funded by the NIH Office of Research Infrastructure Programs (P40 OD010440). Research yielding these results has received funding from the Deutsche Forschungsgemeinschaft (DFG, German Research Foundation) under Germany's Excellence Strategy within the framework of the Munich Cluster for Systems Neurology (EXC 2145 SyNergy—ID 390857198) (F.U.H.) and from the European Research Council (ERC Advanced Grant 101052783—INSITUFOLD).

AUTHOR CONTRIBUTIONS

M.B.D.M. planned and performed all the experiments and analyzed the data with help of G.G.J. M.B.D.M., G.G.J., and F.U.H. conceived the project and participated in data interpretation. P.K. generated the YFP-UTR, YFP-STOP, and HSP-16.1-RFP *C. elegans* reporter strains and helped with initial experiments. P.K. and G.G.J. acted as a co-supervisors. M.B.D.M., G.G.J., and F.U.H. wrote the manuscript.

DECLARATION OF INTERESTS

The authors declare no competing interests.

INCLUSION AND DIVERSITY

We support inclusive, diverse, and equitable conduct of research.

Received: September 30, 2022
Revised: May 17, 2023
Accepted: May 24, 2023
Published: June 19, 2023

REFERENCES

1. Schuller, A.P., and Green, R. (2018). Roadblocks and resolutions in eukaryotic translation. Nat. Rev. Mol. Cell Biol. *19*, 526–541. https://doi.org/10.1038/s41580-018-0011-4.
2. Wolin, S.L., and Maquat, L.E. (2019). Cellular RNA surveillance in health and disease. Science *366*, 822–827. https://doi.org/10.1126/science.aax2957.
3. López-Otín, C., Blasco, M.A., Partridge, L., Serrano, M., and Kroemer, G. (2013). The hallmarks of aging. Cell *153*, 1194–1217. https://doi.org/10.1016/j.cell.2013.05.039.
4. Steffen, K.K., and Dillin, A. (2016). A ribosomal perspective on proteostasis and aging. Cell Metab. *23*, 1004–1012. https://doi.org/10.1016/j.cmet.2016.05.013.
5. Stein, K.C., Morales-Polanco, F., van der Lienden, J., Rainbolt, T.K., and Frydman, J. (2022). Ageing exacerbates ribosome pausing to disrupt cotranslational proteostasis. Nature *601*, 637–642. https://doi.org/10.1038/s41586-021-04295-4.
6. Hipp, M.S., Kasturi, P., and Hartl, F.U. (2019). The proteostasis network and its decline in ageing. Nat. Rev. Mol. Cell Biol. *20*, 421–435. https://doi.org/10.1038/s41580-019-0101-y.
7. Labbadia, J., and Morimoto, R.I. (2015). The biology of proteostasis in aging and disease. Annu. Rev. Biochem. *84*, 435–464. https://doi.org/10.1146/annurev-biochem-060614-033955.
8. Balch, W.E., Morimoto, R.I., Dillin, A., and Kelly, J.W. (2008). Adapting proteostasis for disease intervention. Science *319*, 916–919. https://doi.org/10.1126/science.1141448.
9. Dunn, J.G., Foo, C.K., Belletier, N.G., Gavis, E.R., and Weissman, J.S. (2013). Ribosome profiling reveals pervasive and regulated stop codon

readthrough in Drosophila melanogaster. eLife *2*, e01179. https://doi.org/10.7554/eLife.01179.

10. Loughran, G., Chou, M.Y., Ivanov, I.P., Jungreis, I., Kellis, M., Kiran, A.M., Baranov, P.V., and Atkins, J.F. (2014). Evidence of efficient stop codon readthrough in four mammalian genes. Nucleic Acids Res. *42*, 8928–8938. https://doi.org/10.1093/nar/gku608.
11. Chen, Y., Sun, T., Bi, Z., Ni, J.Q., Pastor-Pareja, J.C., and Javid, B. (2020). Premature termination codon readthrough in Drosophila varies in a developmental and tissue-specific manner. Sci. Rep. *10*, 8485. https://doi.org/10.1038/s41598-020-65348-8.
12. Joazeiro, C.A.P. (2019). Mechanisms and functions of ribosome-associated protein quality control. Nat. Rev. Mol. Cell Biol. *20*, 368–383. https://doi.org/10.1038/s41580-019-0118-2.
13. Sitron, C.S., and Brandman, O. (2020). Detection and degradation of stalled nascent chains via ribosome-associated quality control. Annu. Rev. Biochem. *89*, 417–442. https://doi.org/10.1146/annurev-biochem-013118-110729.
14. Klauer, A.A., and van Hoof, A. (2012). Degradation of mRNAs that lack a stop codon: a decade of nonstop progress. Wiley Interdiscip. Rev. RNA *3*, 649–660. https://doi.org/10.1002/wrna.1124.
15. Schmidt, C., Kowalinski, E., Shanmuganathan, V., Defenouillère, Q., Braunger, K., Heuer, A., Pech, M., Namane, A., Berninghausen, O., Fromont-Racine, M., et al. (2016). The cryo-EM structure of a ribosome-Ski2-Ski3-Ski8 helicase complex. Science *354*, 1431–1433. https://doi.org/10.1126/science.aaf7520.
16. Shibata, N., Ohoka, N., Sugaki, Y., Onodera, C., Inoue, M., Sakuraba, Y., Takakura, D., Hashii, N., Kawasaki, N., Gondo, Y., and Naito, M. (2015). Degradation of stop codon read-through mutant proteins via the ubiquitin-proteasome system causes hereditary disorders. J. Biol. Chem. *290*, 28428–28437. https://doi.org/10.1074/jbc.M115.670901.
17. Rebelo, A.P., Abrams, A.J., Cottenie, E., Horga, A., Gonzalez, M., Bis, D.M., Sanchez-Mejias, A., Pinto, M., Buglo, E., Markel, K., et al. (2016). Cryptic amyloidogenic elements in the 3′ UTRs of neurofilament genes trigger axonal neuropathy. Am. J. Hum. Genet. *98*, 597–614. https://doi.org/10.1016/j.ajhg.2016.02.022.
18. Bock, A.S., Günther, S., Mohr, J., Goldberg, L.V., Jahic, A., Klisch, C., Hübner, C.A., Biskup, S., and Beetz, C. (2018). A nonstop variant in REEP1 causes peripheral neuropathy by unmasking a 3′UTR-encoded, aggregation-inducing motif. Hum. Mutat. *39*, 193–196. https://doi.org/10.1002/humu.23369.
19. Arribere, J.A., Cenik, E.S., Jain, N., Hess, G.T., Lee, C.H., Bassik, M.C., and Fire, A.Z. (2016). Translation readthrough mitigation. Nature *534*, 719–723. https://doi.org/10.1038/nature18308.
20. Dhamija, S., Yang, C.M., Seiler, J., Myacheva, K., Caudron-Herger, M., Wieland, A., Abdelkarim, M., Sharma, Y., Riester, M., Groß, M., et al. (2020). A pan-cancer analysis reveals nonstop extension mutations causing SMAD4 tumour suppressor degradation. Nat. Cell Biol. *22*, 999–1010. https://doi.org/10.1038/s41556-020-0551-7.
21. Kramarski, L., and Arbely, E. (2020). Translational read-through promotes aggregation and shapes stop codon identity. Nucleic Acids Res. *48*, 3747–3760. https://doi.org/10.1093/nar/gkaa136.
22. Yordanova, M.M., Loughran, G., Zhdanov, A.V., Mariotti, M., Kiniry, S.J., O'Connor, P.B.F., Andreev, D.E., Tzani, I., Saffert, P., Michel, A.M., et al. (2018). AMD1 mRNA employs ribosome stalling as a mechanism for molecular memory formation. Nature *553*, 356–360. https://doi.org/10.1038/nature25174.
23. Hashimoto, S., Nobuta, R., Izawa, T., and Inada, T. (2019). Translation arrest as a protein quality control system for aberrant translation of the 3′-UTR in mammalian cells. FEBS Lett. *593*, 777–787. https://doi.org/10.1002/1873-3468.13362.
24. Guna, A., and Hegde, R.S. (2018). Transmembrane domain recognition during membrane protein biogenesis and quality control. Curr. Biol. *28*, R498–R511. https://doi.org/10.1016/j.cub.2018.02.004.
25. Shao, S., Rodrigo-Brenni, M.C., Kivlen, M.H., and Hegde, R.S. (2017). Mechanistic basis for a molecular triage reaction. Science *355*, 298–302. https://doi.org/10.1126/science.aah6130.
26. Sattlegger, E., and Hinnebusch, A.G. (2005). Polyribosome binding by GCN1 is required for full activation of eukaryotic translation initiation factor 2α kinase GCN2 during amino acid starvation. J. Biol. Chem. *280*, 16514–16521. https://doi.org/10.1074/jbc.M414566200.
27. Pakos-Zebrucka, K., Koryga, I., Mnich, K., Ljujic, M., Samali, A., and Gorman, A.M. (2016). The integrated stress response. EMBO Rep. *17*, 1374–1395. https://doi.org/10.15252/embr.201642195.
28. Yan, L.L., and Zaher, H.S. (2021). Ribosome quality control antagonizes the activation of the integrated stress response on colliding ribosomes. Mol. Cell *81*, 614–628.e4. https://doi.org/10.1016/j.molcel.2020.11.033.
29. Wu, C.C., Peterson, A., Zinshteyn, B., Regot, S., and Green, R. (2020). Ribosome collisions trigger general stress responses to regulate cell fate. Cell *182*, 404–416.e14. https://doi.org/10.1016/j.cell.2020.06.006.
30. Pochopien, A.A., Beckert, B., Kasvandik, S., Berninghausen, O., Beckmann, R., Tenson, T., and Wilson, D.N. (2021). Structure of Gcn1 bound to stalled and colliding 80S ribosomes. Proc. Natl. Acad. Sci. USA *118*, e2022756118. https://doi.org/10.1073/pnas.2022756118.
31. Hessa, T., Sharma, A., Mariappan, M., Eshleman, H.D., Gutierrez, E., and Hegde, R.S. (2011). Protein targeting and degradation are coupled for elimination of mislocalized proteins. Nature *475*, 394–397. https://doi.org/10.1038/nature10181.
32. Hsu, A.L., Murphy, C.T., and Kenyon, C. (2003). Regulation of aging and age-related disease by DAF-16 and heat-shock factor. Science *300*, 1142–1145. https://doi.org/10.1126/science.1083701.
33. Walker, G.A., and Lithgow, G.J. (2003). Lifespan extension in C. elegans by a molecular chaperone dependent upon insulin-like signals. Aging Cell *2*, 131–139. https://doi.org/10.1046/j.1474-9728.2003.00045.x.
34. Morley, J.F., and Morimoto, R.I. (2004). Regulation of longevity in Caenorhabditis elegans by heat shock factor and molecular chaperones. Mol. Biol. Cell *15*, 657–664. https://doi.org/10.1091/mbc.e03-07-0532.
35. Walther, D.M., Kasturi, P., Zheng, M., Pinkert, S., Vecchi, G., Ciryam, P., Morimoto, R.I., Dobson, C.M., Vendruscolo, M., Mann, M., and Hartl, F.U. (2015). Widespread proteome remodeling and aggregation in aging C. elegans. Cell *161*, 919–932. https://doi.org/10.1016/j.cell.2015.03.032.
36. Rodrigo-Brenni, M.C., Gutierrez, E., and Hegde, R.S. (2014). Cytosolic quality control of mislocalized proteins requires RNF126 recruitment to Bag6. Mol. Cell *55*, 227–237. https://doi.org/10.1016/j.molcel.2014.05.025.
37. Varshavsky, A. (2019). N-degron and C-degron pathways of protein degradation. Proc. Natl. Acad. Sci. USA *116*, 358–366. https://doi.org/10.1073/pnas.1816596116.
38. Käll, L., Krogh, A., and Sonnhammer, E.L. (2007). Advantages of combined transmembrane topology and signal peptide prediction–the Phobius web server. Nucleic Acids Res. *35*, W429–W432. https://doi.org/10.1093/nar/gkm256.
39. Prilusky, J., and Bibi, E. (2009). Studying membrane proteins through the eyes of the genetic code revealed a strong uracil bias in their coding mRNAs. Proc. Natl. Acad. Sci. USA *106*, 6662–6666. https://doi.org/10.1073/pnas.0902029106.
40. Arribere, J.A., and Fire, A.Z. (2018). Nonsense mRNA suppression via nonstop decay. eLife *7*, e33292. https://doi.org/10.7554/eLife.33292.
41. van Hoof, A., Frischmeyer, P.A., Dietz, H.C., and Parker, R. (2002). Exosome-mediated recognition and degradation of mRNAs lacking a termination codon. Science *295*, 2262–2264. https://doi.org/10.1126/science.1067272.
42. Frischmeyer, P.A., van Hoof, A., O'Donnell, K., Guerrerio, A.L., Parker, R., and Dietz, H.C. (2002). An mRNA surveillance mechanism that eliminates transcripts lacking termination codons. Science *295*, 2258–2261. https://doi.org/10.1126/science.1067338.

43. Theil, K., Imami, K., and Rajewsky, N. (2019). Identification of proteins and miRNAs that specifically bind an mRNA in vivo. Nat. Commun. *10*, 4205. https://doi.org/10.1038/s41467-019-12050-7.

44. Collart, M.A. (2016). The Ccr4-Not complex is a key regulator of eukaryotic gene expression. Wiley Interdiscip. Rev. RNA *7*, 438–454. https://doi.org/10.1002/wrna.1332.

45. Webster, M.W., Chen, Y.H., Stowell, J.A.W., Alhusaini, N., Sweet, T., Graveley, B.R., Coller, J., and Passmore, L.A. (2018). mRNA deadenylation is coupled to translation rates by the differential activities of Ccr4-Not nucleases. Mol. Cell *70*, 1089–1100.e8. https://doi.org/10.1016/j.molcel.2018.05.033.

46. Buschauer, R., Matsuo, Y., Sugiyama, T., Chen, Y.H., Alhusaini, N., Sweet, T., Ikeuchi, K., Cheng, J., Matsuki, Y., Nobuta, R., et al. (2020). The Ccr4-Not complex monitors the translating ribosome for codon optimality. Science *368*, eaay6912. https://doi.org/10.1126/science.aay6912.

47. Nukazuka, A., Fujisawa, H., Inada, T., Oda, Y., and Takagi, S. (2008). Semaphorin controls epidermal morphogenesis by stimulating mRNA translation via eIF2alpha in Caenorhabditis elegans. Genes Dev. *22*, 1025–1036. https://doi.org/10.1101/gad.1644008.

48. Sattlegger, E., and Hinnebusch, A.G. (2000). Separate domains in GCN1 for binding protein kinase GCN2 and ribosomes are required for GCN2 activation in amino acid-starved cells. EMBO J. *19*, 6622–6633. https://doi.org/10.1093/emboj/19.23.6622.

49. Yamazaki, H., Kasai, S., Mimura, J., Ye, P., Inose-Maruyama, A., Tanji, K., Wakabayashi, K., Mizuno, S., Sugiyama, F., Takahashi, S., et al. (2020). Ribosome binding protein GCN1 regulates the cell cycle and cell proliferation and is essential for the embryonic development of mice. PLoS Genet. *16*, e1008693. https://doi.org/10.1371/journal.pgen.1008693.

50. Oltion, K., Carelli, J.D., Yang, T., See, S.K., Wang, H.Y., Kampmann, M., and Taunton, J. (2023). An E3 ligase network engages GCN1 to promote the degradation of translation factors on stalled ribosomes. Cell *186*, 346–362.e17. https://doi.org/10.1016/j.cell.2022.12.025.

51. Coller, J.M., Tucker, M., Sheth, U., Valencia-Sanchez, M.A., and Parker, R. (2001). The DEAD box helicase, Dhh1p, functions in mRNA decapping and interacts with both the decapping and deadenylase complexes. RNA *7*, 1717–1727. https://doi.org/10.1017/s135583820101994x.

52. Passmore, L.A., and Coller, J. (2022). Roles of mRNA poly(A) tails in regulation of eukaryotic gene expression. Nat. Rev. Mol. Cell Biol. *23*, 93–106. https://doi.org/10.1038/s41580-021-00417-y.

53. Han, P., Shichino, Y., Schneider-Poetsch, T., Mito, M., Hashimoto, S., Udagawa, T., Kohno, K., Yoshida, M., Mishima, Y., Inada, T., and Iwasaki, S. (2020). Genome-wide survey of ribosome collision. Cell Rep. *31*, 107610. https://doi.org/10.1016/j.celrep.2020.107610.

54. Zhao, T., Chen, Y.M., Li, Y., Wang, J., Chen, S., Gao, N., and Qian, W. (2021). Disome-seq reveals widespread ribosome collisions that promote cotranslational protein folding. Genome Biol. *22*, 16. https://doi.org/10.1186/s13059-020-02256-0.

55. Meydan, S., and Guydosh, N.R. (2020). Disome and trisome profiling reveal genome-wide targets of ribosome quality control. Mol. Cell *79*, 588–602.e6. https://doi.org/10.1016/j.molcel.2020.06.010.

56. Arpat, A.B., Liechti, A., De Matos, M., Dreos, R., Janich, P., and Gatfield, D. (2020). Transcriptome-wide sites of collided ribosomes reveal principles of translational pausing. Genome Res. *30*, 985–999. https://doi.org/10.1101/gr.257741.119.

57. Oh, E., Becker, A.H., Sandikci, A., Huber, D., Chaba, R., Gloge, F., Nichols, R.J., Typas, A., Gross, C.A., Kramer, G., et al. (2011). Selective ribosome profiling reveals the cotranslational chaperone action of trigger factor in vivo. Cell *147*, 1295–1308. https://doi.org/10.1016/j.cell.2011.10.044.

58. Becker, A.H., Oh, E., Weissman, J.S., Kramer, G., and Bukau, B. (2013). Selective ribosome profiling as a tool for studying the interaction of chaperones and targeting factors with nascent polypeptide chains and ribosomes. Nat. Protoc. *8*, 2212–2239. https://doi.org/10.1038/nprot.2013.133.

59. Matsuo, Y., and Inada, T. (2021). The ribosome collision sensor Hel2 functions as preventive quality control in the secretory pathway. Cell Rep. *34*, 108877. https://doi.org/10.1016/j.celrep.2021.108877.

60. McGlincy, N.J., and Ingolia, N.T. (2017). Transcriptome-wide measurement of translation by ribosome profiling. Methods *126*, 112–129. https://doi.org/10.1016/j.ymeth.2017.05.028.

61. Stein, K.C., Kriel, A., and Frydman, J. (2019). Nascent polypeptide domain topology and elongation rate direct the cotranslational hierarchy of Hsp70 and TRiC/CCT. Mol. Cell *75*, 1117–1130.e5. https://doi.org/10.1016/j.molcel.2019.06.036.

62. Saidijam, M., Azizpour, S., and Patching, S.G. (2018). Comprehensive analysis of the numbers, lengths and amino acid compositions of transmembrane helices in prokaryotic, eukaryotic and viral integral membrane proteins of high-resolution structure. J. Biomol. Struct. Dyn. *36*, 443–464. https://doi.org/10.1080/07391102.2017.1285725.

63. Ito, K., and Chiba, S. (2013). Arrest peptides: cis-acting modulators of translation. Annu. Rev. Biochem. *82*, 171–202. https://doi.org/10.1146/annurev-biochem-080211-105026.

64. Phillips, B.P., and Miller, E.A. (2020). Ribosome-associated quality control of membrane proteins at the endoplasmic reticulum. J. Cell Sci. *133*, jcs251983. https://doi.org/10.1242/jcs.251983.

65. Juszkiewicz, S., Chandrasekaran, V., Lin, Z., Kraatz, S., Ramakrishnan, V., and Hegde, R.S. (2018). ZNF598 is a quality control sensor of collided ribosomes. Mol. Cell *72*, 469–481.e7. https://doi.org/10.1016/j.molcel.2018.08.037.

66. Malhotra, V., and Erlmann, P. (2015). The pathway of collagen secretion. Annu. Rev. Cell Dev. Biol. *31*, 109–124. https://doi.org/10.1146/annurev-cellbio-100913-013002.

67. Kadler, K.E., Baldock, C., Bella, J., and Boot-Handford, R.P. (2007). Collagens at a glance. J. Cell Sci. *120*, 1955–1958. https://doi.org/10.1242/jcs.03453.

68. Ewald, C.Y., Landis, J.N., Porter Abate, J., Murphy, C.T., and Blackwell, T.K. (2015). Dauer-independent insulin/IGF-1-signalling implicates collagen remodelling in longevity. Nature *519*, 97–101. https://doi.org/10.1038/nature14021.

69. Ferraz, R.C., Camara, H., De-Souza, E.A., Pinto, S., Pinca, A.P., Silva, R.C., Sato, V.N., Castilho, B.A., and Mori, M.A. (2016). Impact is a GCN2 inhibitor that limits lifespan in Caenorhabditis elegans. BMC Biol. *14*, 87. https://doi.org/10.1186/s12915-016-0301-2.

70. Krane, S.M. (2008). The importance of proline residues in the structure, stability and susceptibility to proteolytic degradation of collagens. Amino Acids *35*, 703–710. https://doi.org/10.1007/s00726-008-0073-2.

71. Peil, L., Starosta, A.L., Lassak, J., Atkinson, G.C., Virumäe, K., Spitzer, M., Tenson, T., Jung, K., Remme, J., and Wilson, D.N. (2013). Distinct XPPX sequence motifs induce ribosome stalling, which is rescued by the translation elongation factor EF-P. Proc. Natl. Acad. Sci. USA *110*, 15265–15270. https://doi.org/10.1073/pnas.1310642110.

72. Schuller, A.P., Wu, C.C., Dever, T.E., Buskirk, A.R., and Green, R. (2017). eIF5A functions globally in translation elongation and termination. Mol. Cell *66*, 194–205.e5. https://doi.org/10.1016/j.molcel.2017.03.003.

73. Manjunath, H., Zhang, H., Rehfeld, F., Han, J., Chang, T.C., and Mendell, J.T. (2019). Suppression of ribosomal pausing by eIF5A is necessary to maintain the fidelity of start codon selection. Cell Rep. *29*, 3134–3146.e6. https://doi.org/10.1016/j.celrep.2019.10.129.

74. Kucukural, A., Yukselen, O., Ozata, D.M., Moore, M.J., and Garber, M. (2019). DEBrowser: interactive differential expression analysis and visualization tool for count data. BMC Genomics *20*, 6. https://doi.org/10.1186/s12864-018-5362-x.

75. Yang, Q., Yu, C.H., Zhao, F., Dang, Y., Wu, C., Xie, P., Sachs, M.S., and Liu, Y. (2019). eRF1 mediates codon usage effects on mRNA translation

efficiency through premature termination at rare codons. Nucleic Acids Res. *47*, 9243–9258. https://doi.org/10.1093/nar/gkz710.

76. Baradaran-Heravi, A., Balgi, A.D., Hosseini-Farahabadi, S., Choi, K., Has, C., and Roberge, M. (2021). Effect of small molecule eRF3 degraders on premature termination codon readthrough. Nucleic Acids Res. *49*, 3692–3708. https://doi.org/10.1093/nar/gkab194.
77. Matyskiela, M.E., Lu, G., Ito, T., Pagarigan, B., Lu, C.C., Miller, K., Fang, W., Wang, N.Y., Nguyen, D., Houston, J., et al. (2016). A novel cereblon modulator recruits GSPT1 to the CRL4(CRBN) ubiquitin ligase. Nature *535*, 252–257. https://doi.org/10.1038/nature18611.
78. Uhlén, M., Fagerberg, L., Hallström, B.M., Lindskog, C., Oksvold, P., Mardinoglu, A., Sivertsson, Å., Kampf, C., Sjöstedt, E., Asplund, A., et al. (2015). Proteomics. Tissue-based map of the human proteome. Science *347*, 1260419. https://doi.org/10.1126/science.1260419.
79. Zeng, F., Li, X., Pires-Alves, M., Chen, X., Hawk, C.W., and Jin, H. (2021). Conserved heterodimeric GTPase Rbg1/Tma46 promotes efficient translation in eukaryotic cells. Cell Rep. *37*, 109877. https://doi.org/10.1016/j.celrep.2021.109877.
80. Sinha, N.K., Ordureau, A., Best, K., Saba, J.A., Zinshteyn, B., Sundaramoorthy, E., Fulzele, A., Garshott, D.M., Denk, T., Thoms, M., et al. (2020). EDF1 coordinates cellular responses to ribosome collisions. eLife *9*, e58828. https://doi.org/10.7554/eLife.58828.
81. Juszkiewicz, S., Slodkowicz, G., Lin, Z., Freire-Pritchett, P., Peak-Chew, S.Y., and Hegde, R.S. (2020). Ribosome collisions trigger cis-acting feedback inhibition of translation initiation. eLife *9*, e60038. https://doi.org/10.7554/eLife.60038.
82. Vind, A.C., Snieckute, G., Blasius, M., Tiedje, C., Krogh, N., Bekker-Jensen, D.B., Andersen, K.L., Nordgaard, C., Tollenaere, M.A.X., Lund, A.H., et al. (2020). ZAKalpha recognizes stalled ribosomes through partially redundant sensor domains. Mol. Cell *78*, 700–713.e7. https://doi.org/10.1016/j.molcel.2020.03.021.
83. Wangen, J.R., and Green, R. (2020). Stop codon context influences genome-wide stimulation of termination codon readthrough by Aminoglycosides. eLife *9*, e52611. https://doi.org/10.7554/eLife.52611.
84. Neumann, T., Herzog, V.A., Muhar, M., von Haeseler, A., Zuber, J., Ameres, S.L., and Rescheneder, P. (2019). Quantification of experimentally induced nucleotide conversions in high-throughput sequencing datasets. BMC Bioinformatics *20*, 258. https://doi.org/10.1186/s12859-019-2849-7.
85. Presnyak, V., Alhusaini, N., Chen, Y.H., Martin, S., Morris, N., Kline, N., Olson, S., Weinberg, D., Baker, K.E., Graveley, B.R., and Coller, J. (2015). Codon optimality is a major determinant of mRNA stability. Cell *160*, 1111–1124. https://doi.org/10.1016/j.cell.2015.02.029.
86. Forrest, M.E., Pinkard, O., Martin, S., Sweet, T.J., Hanson, G., and Coller, J. (2020). Codon and amino acid content are associated with mRNA stability in mammalian cells. PLoS One *15*, e0228730. https://doi.org/10.1371/journal.pone.0228730.
87. Wu, Q., Medina, S.G., Kushawah, G., DeVore, M.L., Castellano, L.A., Hand, J.M., Wright, M., and Bazzini, A.A. (2019). Translation affects mRNA stability in a codon-dependent manner in human cells. eLife *8*, e45396. https://doi.org/10.7554/eLife.45396.
88. Leznicki, P., and High, S. (2020). SGTA associates with nascent membrane protein precursors. EMBO Rep. *21*, e48835. https://doi.org/10.15252/embr.201948835.
89. Farkas, Á., and Bohnsack, K.E. (2021). Capture and delivery of tail-anchored proteins to the endoplasmic reticulum. J. Cell Biol. *220*, e202105004. https://doi.org/10.1083/jcb.202105004.
90. Leznicki, P., and High, S. (2012). SGTA antagonizes BAG6-mediated protein triage. Proc. Natl. Acad. Sci. USA *109*, 19214–19219. https://doi.org/10.1073/pnas.1209997109.
91. Mariappan, M., Li, X., Stefanovic, S., Sharma, A., Mateja, A., Keenan, R.J., and Hegde, R.S. (2010). A ribosome-associating factor chaperones tail-anchored membrane proteins. Nature *466*, 1120–1124. https://doi.org/10.1038/nature09296.
92. Mogk, A., and Bukau, B. (2017). Role of sHsps in organizing cytosolic protein aggregation and disaggregation. Cell Stress Chaperones *22*, 493–502. https://doi.org/10.1007/s12192-017-0762-4.
93. Haslbeck, M., Weinkauf, S., and Buchner, J. (2019). Small heat shock proteins: simplicity meets complexity. J. Biol. Chem. *294*, 2121–2132. https://doi.org/10.1074/jbc.REV118.002809.
94. Kesner, J.S., Chen, Z., Shi, P., Aparicio, A.O., Murphy, M.R., Guo, Y., Trehan, A., Lipponen, J.E., Recinos, Y., Myeku, N., and Wu, X. (2023). Noncoding translation mitigation. Nature *617*, 395–402. https://doi.org/10.1038/s41586-023-05946-4.
95. Hanson, G., and Coller, J. (2018). Codon optimality, bias and usage in translation and mRNA decay. Nat. Rev. Mol. Cell Biol. *19*, 20–30. https://doi.org/10.1038/nrm.2017.91.
96. Mishima, Y., Han, P., Ishibashi, K., Kimura, S., and Iwasaki, S. (2022). Ribosome slowdown triggers codon-mediated mRNA decay independently of ribosome quality control. EMBO J. *41*, e109256. https://doi.org/10.15252/embj.2021109256.
97. Rodnina, M.V., and Wintermeyer, W. (2016). Protein elongation, co-translational folding and targeting. J. Mol. Biol. *428*, 2165–2185. https://doi.org/10.1016/j.jmb.2016.03.022.
98. Pechmann, S., Chartron, J.W., and Frydman, J. (2014). Local slowdown of translation by nonoptimal codons promotes nascent-chain recognition by SRP in vivo. Nat. Struct. Mol. Biol. *21*, 1100–1105. https://doi.org/10.1038/nsmb.2919.
99. Miller-Vedam, L.E., Bräuning, B., Popova, K.D., Schirle Oakdale, N.T., Bonnar, J.L., Prabu, J.R., Boydston, E.A., Sevillano, N., Shurtleff, M.J., Stroud, R.M., et al. (2020). Structural and mechanistic basis of the EMC-dependent biogenesis of distinct transmembrane clients. eLife *9*, e62611. https://doi.org/10.7554/eLife.62611.
100. O'Donnell, J.P., Phillips, B.P., Yagita, Y., Juszkiewicz, S., Wagner, A., Malinverni, D., Keenan, R.J., Miller, E.A., and Hegde, R.S. (2020). The architecture of EMC reveals a path for membrane protein insertion. eLife *9*, e57887. https://doi.org/10.7554/eLife.57887.
101. Trentini, D.B., Pecoraro, M., Tiwary, S., Cox, J., Mann, M., Hipp, M.S., and Hartl, F.U. (2020). Role for ribosome-associated quality control in sampling proteins for MHC class I-mediated antigen presentation. Proc. Natl. Acad. Sci. USA *117*, 4099–4108. https://doi.org/10.1073/pnas.1914401117.
102. Tector, M., and Hartl, F.U. (1999). An unstable transmembrane segment in the cystic fibrosis transmembrane conductance regulator. EMBO J. *18*, 6290–6298. https://doi.org/10.1093/emboj/18.22.6290.
103. Smalinskaitė, L., Kim, M.K., Lewis, A.J.O., Keenan, R.J., and Hegde, R.S. (2022). Mechanism of an intramembrane chaperone for multipass membrane proteins. Nature *611*, 161–166. https://doi.org/10.1038/s41586-022-05336-2.
104. Sundaram, A., Yamsek, M., Zhong, F., Hooda, Y., Hegde, R.S., and Keenan, R.J. (2022). Substrate-driven assembly of a translocon for multipass membrane proteins. Nature *611*, 167–172. https://doi.org/10.1038/s41586-022-05330-8.
105. Shoulders, M.D., and Raines, R.T. (2009). Collagen structure and stability. Annu. Rev. Biochem. *78*, 929–958. https://doi.org/10.1146/annurev.biochem.77.032207.120833.
106. Onursal, C., Dick, E., Angelidis, I., Schiller, H.B., and Staab-Weijnitz, C.A. (2021). Collagen biosynthesis, processing, and maturation in lung ageing. Front. Med. (Lausanne) *8*, 593874. https://doi.org/10.3389/fmed.2021.593874.
107. Pavlov, M.Y., Watts, R.E., Tan, Z., Cornish, V.W., Ehrenberg, M., and Forster, A.C. (2009). Slow peptide bond formation by proline and other N-alkylamino acids in translation. Proc. Natl. Acad. Sci. USA *106*, 50–54. https://doi.org/10.1073/pnas.0809211106.

108. Gutierrez, E., Shin, B.S., Woolstenhulme, C.J., Kim, J.R., Saini, P., Buskirk, A.R., and Dever, T.E. (2013). eIF5A promotes translation of polyproline motifs. Mol. Cell *51*, 35–45. https://doi.org/10.1016/j.molcel.2013.04.021.

109. Kulak, N.A., Pichler, G., Paron, I., Nagaraj, N., and Mann, M. (2014). Minimal, encapsulated proteomic-sample processing applied to copy-number estimation in eukaryotic cells. Nat. Methods *11*, 319–324. https://doi.org/10.1038/nmeth.2834.

110. Shcherbakov, D., Nigri, M., Akbergenov, R., Brilkova, M., Mantovani, M., Petit, P.I., Grimm, A., Karol, A.A., Teo, Y., Sanchón, A.C., et al. (2022). Premature aging in mice with error-prone protein synthesis. Sci. Adv. *8*, eabl9051. https://doi.org/10.1126/sciadv.abl9051.

111. Moore, J., Akbergenov, R., Nigri, M., Isnard-Petit, P., Grimm, A., Seebeck, P., Restelli, L., Frank, S., Eckert, A., Thiam, K., et al. (2021). Random errors in protein synthesis activate an age-dependent program of muscle atrophy in mice. Commun. Biol. *4*, 703. https://doi.org/10.1038/s42003-021-02204-z.

112. Azpurua, J., Ke, Z., Chen, I.X., Zhang, Q., Ermolenko, D.N., Zhang, Z.D., Gorbunova, V., and Seluanov, A. (2013). Naked mole-rat has increased translational fidelity compared with the mouse, as well as a unique 28S ribosomal RNA cleavage. Proc. Natl. Acad. Sci. USA *110*, 17350–17355. https://doi.org/10.1073/pnas.1313473110.

113. Ito, S., and Nagata, K. (2021). Quality control of procollagen in cells. Annu. Rev. Biochem. *90*, 631–658. https://doi.org/10.1146/annurev-biochem-013118-111603.

114. Paix, A., Folkmann, A., Rasoloson, D., and Seydoux, G. (2015). High efficiency, homology-directed genome editing in Caenorhabditis elegans using CRISPR-Cas9 ribonucleoprotein complexes. Genetics *201*, 47–54. https://doi.org/10.1534/genetics.115.179382.

115. Chu, C., Quinn, J., and Chang, H.Y. (2012). Chromatin isolation by RNA purification (ChIRP). J. Vis. Exp.3912 https://doi.org/10.3791/3912.

116. Ran, F.A., Hsu, P.D., Wright, J., Agarwala, V., Scott, D.A., and Zhang, F. (2013). Genome engineering using the CRISPR-Cas9 system. Nat. Protoc. *8*, 2281–2308. https://doi.org/10.1038/nprot.2013.143.

117. Sitron, C.S., and Brandman, O. (2019). CAT tails drive degradation of stalled polypeptides on and off the ribosome. Nat. Struct. Mol. Biol. *26*, 450–459. https://doi.org/10.1038/s41594-019-0230-1.

118. Livak, K.J., and Schmittgen, T.D. (2001). Analysis of relative gene expression data using real-time quantitative PCR and the 2(-Delta Delta C(T)) Method. Methods *25*, 402–408. https://doi.org/10.1006/meth.2001.1262.

119. Lauria, F., Tebaldi, T., Bernabò, P., Groen, E.J.N., Gillingwater, T.H., and Viero, G. (2018). riboWaltz: optimization of ribosome P-site positioning in ribosome profiling data. PLoS Comput. Biol. *14*, e1006169. https://doi.org/10.1371/journal.pcbi.1006169.

120. Love, M.I., Huber, W., and Anders, S. (2014). Moderated estimation of fold change and dispersion for RNA-seq data with DESeq2. Genome Biol. *15*, 550. https://doi.org/10.1186/s13059-014-0550-8.

121. Li, F., Xing, X., Xiao, Z., Xu, G., and Yang, X. (2020). RiboMiner: a toolset for mining multi-dimensional features of the translatome with ribosome profiling data. BMC Bioinformatics *21*, 340. https://doi.org/10.1186/s12859-020-03670-8.

122. Liao, Y., Smyth, G.K., and Shi, W. (2014). featureCounts: an efficient general purpose program for assigning sequence reads to genomic features. Bioinformatics *30*, 923–930. https://doi.org/10.1093/bioinformatics/btt656.

123. Herzog, V.A., Reichholf, B., Neumann, T., Rescheneder, P., Bhat, P., Burkard, T.R., Wlotzka, W., von Haeseler, A., Zuber, J., and Ameres, S.L. (2017). Thiol-linked alkylation of RNA to assess expression dynamics. Nat. Methods *14*, 1198–1204. https://doi.org/10.1038/nmeth.4435.

124. Wu, X., and Bartel, D.P. (2017). kpLogo: positional k-mer analysis reveals hidden specificity in biological sequences. Nucleic Acids Research *45*, W534–W538. https://doi.org/10.1093/nar/gkx323.

STAR★METHODS

KEY RESOURCES TABLE

REAGENT or RESOURCE	SOURCE	IDENTIFIER
Antibodies		
BAG6	Santa Cruz	sc-365928 RRID: AB_10920223
SGTA	Cell Signal	3349S RRID: AB_2188828
RNF126	Abcam	ab234812
RNF115	Abcam	ab187642
GCN1 (immunoblot)	Sigma	HPA019648 RRID: AB_1849567
GCN1 (selective riboseq)	Thermo Fisher	A301-843A RRID: AB_1264319
GFP antibody	Roche	11814460001 RRID: AB_390913
α-tubulin	Merck	T6199 RRID: AB_477583
P-eIF2α	Abcam	ab32157 RRID: AB_732117
P-p38 MAPK	Cell Signaling	9211S RRID: AB_331641
eRF3	Abcam	ab126090 RRID: AB_11128263
eRF1	Santa Cruz	sc-365686 RRID: AB_10843214
Chemicals and reagents		
Dynabeads protein G	Thermo Fisher	10003D
Dynabeads MyOne Streptavidin C1	Thermo Fisher	65001
GFP-trap magnetic agarose	Chromotek	gtma
Anti-FLAG® M2 magnetic beads	Sigma	M8823
Cycloheximide	Sigma	01810
CC-885	MedChemExpress	HY-101488
G418	Thermo Fisher	10131035
RIPA	Thermo Fisher	89900
PhosSTOP	Roche	4906837001
cOmplete, EDTA-free Protease Inhibitor Cocktail	Roche	11873580001
T4 PNK	NEB	M0201S
15% TBE-Urea gel	Thermo Fisher	EC68852BOX
T4 Rnl2(tr) K227Q	NEB	M0351L
riboPOOLs (C. elegans)	siTOOLs/Biozym	27DP-K024-000067
riboPOOLs (H. sapiens)	siTOOLs/Biozym	27DP-K024-000042
Protoscript II reverse transcriptase	NEB	M0368L
Phusion polymerase	NEB	M0530L
CircLigase I	Biozym	131401
8% TBE gel	Thermo Fisher	EC62155BOX
microRNA marker	NEB	N2102S
RNAseI	Biozym	N6901K
DMEM	Thermo Fisher	11995073

(*Continued on next page*)

Continued

REAGENT or RESOURCE	SOURCE	IDENTIFIER
FBS	Gibco	10270106
Lipofectamine 3000	Thermo Fisher	L3000008
Lysozyme	Sigma	L6876
HisTrap Hp column	GE Healthcare	17-5247-01
26/60 Sephacryl S-200 column	GE Healthcare	17-1195-01
Amicon 100K filter	Milipore	UFC910024
iST 8x kit	Preomics	P.O.00001
0.5 ml open-top thickwall polycarbonate tubes	Beckman Coulter	343776
SLAMseq Kinetics Kit	Lexogen	062.24
QuantSeq 3′ mRNA-Seq Library Prep Kit	Lexogen	015.24
QuantiTect Reverse Transcription Kit	Qiagen	205311
SYBR Green PCR Master Mix	Thermo Fisher	4309155
NEBNext Ultra II Directional RNA Library Prep Kit	NEB	E7765
NEBNext Poly(A) mRNA Magnetic Isolation Module	NEB	E7490
SUPERase*In	Invitrogen	AM2694
Trizol	Invitrogen	15596026
NuPAGE 4%–12% Bis-Tris SDS gels	Invitrogen	NP0335BOX
NuPAGE MOPS SDS running buffer	Invitrogen	NP0002
Puromycin	Thermo Fisher	A1113803
Recombinant DNA		
unc-54p::YFP-STOP	This study	pPK86
unc-54p::YFP-UTR	This study	pPK89
unc-54p::mScarlet-T2A-YFP (NotI) myo-3p::CFP	This study	pMM23
unc-54p::mScarlet-T2A-YFP-slc-17.5(3UTR) myo-3p::CFP	This study	pMM24
unc-54p::mScarlet-T2A-YFP- F40D4.17(3UTR) myo-3p::CFP	This study	pMM25
unc-54p::mScarlet-T2A-YFP-R160.3(3UTR) myo-3p::CFP	This study	pMM26
unc-54p::mScarlet-T2A-YFP- T21C12.3(3UTR) myo-3p::CFP	This study	pMM27
unc-54p::mScarlet-T2A-YFP-sec-61.b myo-3p::CFP	This study	pMM28
unc-54p::mScarlet-T2A-YFP-sec-61.b(TA) myo-3p::CFP	This study	pMM29
unc-54p::mScarlet-T2A-YFP-STOP-slc-17.5(3UTR) myo-3p::CFP	This study	pMM30
unc-54p::mScarlet-T2A-YFP-STOP-F40D4.17(3UTR) myo-3p::CFP	This study	pMM31
unc-54p::mScarlet-T2A-YFP-STOP-R160.3(3UTR) myo-3p::CFP	This study	pMM32
unc-54p::mScarlet-T2A-YFP-STOP- T21C12.3(3UTR) myo-3p::CFP	This study	pMM33
unc-54p::mScarlet-T2A-YFP-STOP-sec-61.b myo-3p::CFP	This study	pMM34
unc-54p::mScarlet-T2A-YFP-STOP-sec-61.b(TA) myo-3p::CFP	This study	pMM35
unc-54p::mScarlet-T2A-T2A-YFP	This study	pMM36
unc-54p::mScarlet-T2A- F40D4.17(3UTR)-T2A-YFP	This study	pMM37
unc-54p::mScarlet-T2A- F40D4.17(3UTR)-T2A-YFP codon optimized 1	This study	pMM38
unc-54p::mScarlet-T2A- F40D4.17(3UTR)-T2A-YFP codon optimized 2	This study	pMM39
unc-54p::mScarlet-T2A- SLC-17.5(3UTR)-T2A-YFP	This study	pMM40
unc-54p::mScarlet-T2A- SLC-17.5(3UTR)-T2A-YFP codon optimized 1	This study	pMM41
unc-54p::mScarlet-T2A- SLC-17.5(3UTR)-T2A-YFP codon optimized 2	This study	pMM42
unc-54p::mScarlet-T2A- K_{20}(AAA)T2A-YFP	This study	pMM43
pCMV-mScarlet-P2A-P2A-EYFP(XbaI) pCMV-mTurq2	This study	pMM44
pCMV-mScarlet-P2A-P2A-EYFP-TCEAL1(3UTR) pCMV-mTurq2	This study	pMM45
pCMV-mScarlet-P2A-P2A-EYFP-(3UTR) pCMV-mTurq2	This study	pMM46
pCMV-mScarlet-P2A-P2A-EYFP-CNIH3(3UTR) pCMV-mTurq2	This study	pMM47
pCMV-mScarlet-P2A-P2A-EYFP-OR8D4(3UTR) pCMV-mTurq2	This study	pMM48
pCMV-mScarlet-P2A-P2A-EYFP-CCK(3UTR) pCMV-mTurq2	This study	pMM49

(*Continued on next page*)

Continued

REAGENT or RESOURCE	SOURCE	IDENTIFIER
pCMV-mScarlet-P2A-P2A-EYFP-SEC-61.B pCMV-mTurq2	This study	pMM50
pCMV-mScarlet-P2A-P2A-EYFP-SEC-61.B(TA) pCMV-mTurq2	This study	pMM51
pCMV-EYFP	This study	pMM52
pCMV-EYFP-TCEAL(3UTR)	This study	pMM53
pCMV-EYFP pCMV-mTurquoise2	This study	pMM54
pCMV-mScarlet pCMV-mTurquoise2	This study	pMM55
pHO4d-Cas9	Addgene	67881
pSpCas9(BB)-2A-Puro (PX459) V2.0	Addgene	62988
Oligonucleotides		
qPCR tba-1 fw: ACCAACAAGCCGATGGAGAA	This study	N/A
qPCR tba-1 rev: ACCACGAGCGTAGTTGTTGG	This study	N/A
qPCR pmp-3 fw:CACTTTCACCGCCCAATGAC	This study	N/A
qPCR pmp-3 rev: TCGACGCCAATGACAATCCA	This study	N/A
qPCR EYFP fw: TGAACTTCAAGATCCGCCACA	This study	N/A
qPCR EYFP rev: TTCTCGTTGGGGTCTTTGCT	This study	N/A
qPCR hsp-16.1 fw: AGATATGGCTCAGATGGAACGTC	This study	N/A
qPCR hsp-16.1 rev: GCTTGAACTGCGAGACATTGAG	This study	N/A
qPCR hsp-16.2 fw: TCCATCTGAGTCTTCTGAGATTGTT	This study	N/A
qPCR hsp-16.2 rev: TGATAGCGTACGACCATCCAAA	This study	N/A
qPCR hsp-16.48 fw: GCTCATGCTCCGTTCTCCAT	This study	N/A
qPCR hsp-16.48 rev: TGAGAAACATCGAGTTGAACAGAGA	This study	N/A
qPCR hsp-70 fw: CCGGTTGAAAAGGCACTTCG	This study	N/A
qPCR hsp-70 rev: GAGCAGTTGAGGTCCTTCCC	This study	N/A
YFP Probe #1 TGAACTTGTGGCCGTTTACG	This study	N/A
YFP Probe #2 TGGTGCAGATGAACTTCAGG	This study	N/A
YFP Probe #3 TAGCCGAAGGTGGTCACGAG	This study	N/A
YFP Probe #4 AAGAAGTCGTGCTGCTTCAT	This study	N/A
YFP Probe #5 CTTGAAGAAGATGGTGCGCT	This study	N/A
YFP Probe #6 TTGAAGTCGATGCCCTTCAG	This study	N/A
YFP Probe #7 TAGACGTTGTGGCTGTTGTA	This study	N/A
YFP Probe #8 CTTGAAGTTCACCTTGATGC	This study	N/A

(*Continued on next page*)

Continued

REAGENT or RESOURCE	SOURCE	IDENTIFIER
YFP Probe #9 TAGCTCAGGTAGTGGTTGTC	This study	N/A
YFP Probe #10 TCGTCCATGCCGAGAGTGAT	This study	N/A
CRISPRevolution sgRNA EZ Kit (modified) sgRNA GCN-1 (Cele): GGGUUACACUUUAUUGAUAG	Synthego	N/A
ssODN GCN-1 3xFLAG repair template attttcagatcattcaacgacgggttacactttattgatagtcgaaaATGgactacaag gacgacgatgacaaggactacaaggacgacgatgacaaggactacaaggacga cgatgacaagTCTGACGATGAAATAAAAAGCGAACATGTTCAG GAGAAGACGGAAAATCT	This study	N/A
3xFLAG GCN-1 screen primer fw: CAGATCATTCAACGACGGGTT	This study	N/A
3xFLAG GCN-1 screen primer rev: ttaggcctcaaaaccgaacCT	This study	N/A
RNF126 sgRNA GAGGCGTCGCCGCATCCCGGA	This study	N/A
GCN1 sgRNA GTGCAAAACGCTTTAGTGTCT	This study	N/A
RNF115 sgRNA GAAAGTGGCAGAAAAACCGGT	This study	N/A
SGTA sgRNA GTCACCCCAAACGCAGTCTCC	This study	N/A
BAG6 sgRNA GACATAGGCCGGACCACATGC	This study	N/A
ON-TARGETplus Human CNOT1 siRNA	Dharmacon	L-015369-01-0005
NI-800 (Upper size monosome marker) 5′-AUGUACACUAGGGAUAACAGGGUAAUCAACGCGA/3Phos/	McGlincy and Ingolia[60]	N/A
NI-801 (Lower size monosome marker) 5′-AUGUUAGGGAUAACAGGGUAAUGCGA/3Phos/	McGlincy and Ingolia[60]	N/A
Disome upper size marker 5′-AUGUACACGGAGUCGAGCACCCGCAACGCGAAUGUACACGGA GUCGAGCACCCGCAACGCGAUGUACA	Meydan and Guydosh[55]	N/A
Disome lower size marker 5′-AUGUACACGGAGUCGAGCACCCGCAACGCGAAUGUACACGGA GUCGAGCACCCG/3Phos/	Meydan and Guydosh[55]	N/A
C. elegans strains		
unc-54p::YFP-STOP	This study	FUH277
unc-54p::YFP-UTR	This study	FUH279
unc-54p::YFP-UTR; rpn-10 (ok1865)	This study	FUH492
unc-54p::YFP-UTR; rnf-126 (gk504603)	This study	FUH432
unc-54p::YFP-UTR; gcn-1 (nc40)	This study	FUH491
unc-54p::YFP-UTR; skih-2 (cc2854)	This study	FUH483
3xFLAG-gcn-1(mar02)	This study	FUH503
skih-2(cc2854) 2x BC	Andrew Fire lab	PD2860
gcn-1(nc40)	CGC	RRID: WB-STRAIN: WBStrain00034488
N2(wild-type)	CGC	RRID: WB-STRAIN: WBStrain00000001
rnf-126(gk504603) 6x BC	CGC	FUH431
Cell lines		
HEK293T	ATCC	RRID: CVCL_0063

(*Continued on next page*)

Continued

REAGENT or RESOURCE	SOURCE	IDENTIFIER
Software, Algorithms and Data availibility		
DEBrowser	https://github.com/UMMS-Biocore/debrowser	N/A
DESeq2	https://github.com/mikelove/DESeq2	N/A
STAR	https://github.com/alexdobin/STAR	N/A
Bowtie2	https://github.com/BenLangmead/bowtie2	N/A
umi_tools	https://github.com/CGATOxford/UMI-tools	N/A
riboWaltz	https://github.com/LabTranslationalArchitectomics/riboWaltz	N/A
RiboMiner	https://github.com/xryanglab/RiboMiner	N/A
Fiji	https://imagej.net/software/fiji/	N/A
Graphpad Prism	https://www.graphpad.com/scientific-software/prism/	N/A
Biopython	https://github.com/biopython/biopython	N/A
kpLogo	http://kplogo.wi.mit.edu/	N/A
Gene Ontology	http://geneontology.org/	N/A
Perseus	https://maxquant.net/perseus/	N/A
MaxQuant	https://maxquant.net/maxquant/	N/A
Proteomic datasets	This study	ProteomeXchange: PXD037037
Immunoblots, Microscopy and Flow cytometry data	This study	https://doi.org/10.17632/8rss6rghvb.2
NGS datasets	This study	GEO: GSE214396

RESOURCE AVAILABILITY

Lead contact

Further information and requests for resources and reagents should be directed to and will be fulfilled by the lead contact, F. Ulrich Hartl (uhartl@biochem.mpg.de).

Materials availability

Plasmids and strains generated in this study are available upon request to the lead contact.

Data and code availability

- Mass spectrometry raw data was deposited at the ProteomeXchange consortium PRIDE with the identifier PXD037037. Sequencing data was uploaded to NCBI's Gene Expression Omnibus and are accessible through GEO series accession number GSE214396. Both datasets are listed in the key resources table. Original immunoblot images have been deposited at Mendeley and are publicly available as of the date of publication. The DOI is listed in the key resources table.
- This paper does not report original code.
- Any additional information required to reanalyze the data reported in this paper is available from the lead contact upon request.

EXPERIMENTAL MODEL AND SUBJECT DETAILS

C. elegans strains and growth conditions

The Bristol strain N2 was used as wild-type. Strains used in this study are listed in the key resources table. Worms were grown on nematode growth medium (NGM) seeded with OP50 bacteria and maintained at 20°C unless otherwise indicated. For liquid culture,

worm eggs were collected by bleaching and synchronized populations of L1 larvae were obtained by overnight growth in M9 medium. The L1 larvae were grown in S Basal in presence of OP50 bacteria. Wild-type (N2) males were produced by transferring hermaphrodites to 30°C for 4-6 h and subsequently returned to 20°C. The offspring were screened for males. To remove background mutations, the wild-type males were crossed with a mutant hermaphrodite. Individual F1 worms were isolated and screened for heterozygotes by single-worm PCR. The offspring of identified heterozygotes were then screened for homozygous nematodes carrying the mutant allele. This process was repeated twice for CRIPSR-generated worm lines and 6 times for strains obtained from CGC.

Cell culture and transfection

HEK293T (ATCC, CRL-3216) cells were cultured in DMEM (Thermo Scientific, 11995073) supplemented with 10% FBS (Gibco, 10270106) at 5% CO_2 and 37°C. Cells were transfected using lipofectamine 3000 (Thermo Scientific) following the manufacturer's instructions. Cells were analyzed 48 h after transfection by flow cytometry.

METHOD DETAILS

Cas9 expression and purification

Cas9 purification was adapted from Paix et al.[114] BL21 (DE3) *E. coli* were transformed with pHO4d-Cas9 (Addgene #67881).[114] The main culture was induced at a density of OD_{600} = 0.8 with a final concentration of 0.2 mM IPTG at 18°C overnight. Cells were collected by centrifugation and 6 ml Buffer A (20 mM Tris pH 8.0, 250 mM KCl, 20 mM Imidazole, 10% glycerol, 1 mM TCEP, 1x cOmplete EDTA-free protease inhibitor) was added per gram of wet culture. Lysozyme was added to a final concentration of 1 mg/ml (Sigma, L6876). The suspension was lysed by sonication on ice (10% amplitude, 1.5 s pulse, 5 s pause) for a total time of 45 min. The lysate was clarified by centrifugation at 16,000 x g and the supernatant transferred to a fresh tube. Clarified lysate was passed over a 5 ml HisTrap Hp column (GE Healthcare) at a flowrate of 0.5 ml/min and washed with 100 ml of buffer B (20 mM Tris pH 8.0, 800 mM KCl, 20 mM imidazole, 10% glycerol, 1mM TCEP). The bound protein was eluted with 20 column volumes of a gradient from 0-100% buffer C (20 mM HEPES pH 8.0, 500 mM KCl, 250 mM imidazole, 10% glycerol). Eluent was passed over a MonoQ column to remove Cas9-bound DNA and the flowthrough was collected. To remove any aggregated Cas9 protein, the flowthrough was separated on a 26/60 Sephacryl S-200 column (GE Healthcare #17-1195-01) with Buffer D (20mM HEPES pH 7.5, 500 mM KCl, 20% glycerol). Fractions containing monomeric Cas9 were pooled and concentrated to 10 mg/ml by centrifugation through a 100K filter (Milipore, UFC910024).

CRISPR/Cas9-mediated homologous recombination

Generation of transgenic animals was performed as previously described with adaptations.[114] Briefly, an aliquot of 5 μl purified Cas9 was thawed on ice and incubated with a 100mer sgRNA (Synthego) targeting the gene of interest and *dpy-10* as an injection control for 10 min at room temperature (RT). For deletions/knockouts ssODNs (synthetic single-stranded oligodeoxynucleotide donors) were ordered from Integrated DNA Technologies (IDT) as a repair template and reconstituted to a concentration of 1 mg/ml for the gene of interest and 0.5 mg/ml for *dpy-10*. After incubation, 2.2 μl of ssODN for the gene of interest and 0.55 μl of ssODN against dpy-10 was added to the injection mix. To keep Cas9 soluble, 0.5 μl of 1 M KCL and 0.75 μl of 200 mM HEPES pH 7.4 was added. The injection mix was topped up to 20 μl with water and centrifuged at 20,000 x g for 2 min before injecting it into the gonads of the nematodes. The injection mix or ribonucleoprotein complexes (protein Cas9, tracrRNA, crRNA) and ssODN were microinjected into the gonad of young adults using standard methods. Single injected worms were placed at 20°C. Integrated lines were identified by screening for rollers and singled out on individual plates.

Immunoblotting

Synchronized D1 adult worms were lysed using a Biorupter (Diagenode) (7 cycles of 30 s on with 30 s pause) at 4°C. Lysate was clarified by centrifugation at 400 x g for 10 min at 4°C. Proteins were transferred from polyacrylamide gels to nitrocellulose membranes (GE Healthcare) at a constant voltage of 75 V, limiting the current to 200 mA for 2 h. Membranes were washed in TBS-T buffer (10 mM Tris-HCl pH 7.5, 150 mM NaCl, 0.05% Tween-20) and blocked with 5% skim milk for 1 h at RT. Membranes were incubated with primary antibody in TBS-T with 5% skim milk overnight at 4°C. The blot was then washed 4 times with TBS-T for 10 min each time at RT and incubated with secondary antibody for 1 h at RT. After 4 washes the blot was developed either on an ImageQuant LAS 4000 or ImageQuant 800 system. Images were analyzed in FIJI.

LC-MS/MS analysis

For mass spectrometry analysis, tryptic peptides were loaded on a reverse phase column with an inner diameter of 75 μm packed with 1.9 μm C18 beads using the autosampler of the Thermo Easy LC system (Thermo Scientific). Temperature of the column was kept at a constant 50°C in a column oven (Sonation). Peptides were loaded in buffer A (0.1% formic acid), separated with a 130 min gradient of 5%–30% buffer B (80% ACN and 0.1% formic acid) at a flowrate of 300 (or 250) nl/min and directly applied onto a benchtop Orbitrap Q Exactive HF mass spectrometer (Thermo Scientific) via electrospray. The Q-Exactive HF was operated in data-dependent mode with survey scans at mass range of 300 to 1650 m/z. Up to the 10 or 15 most abundant precursor patterns from the survey

scan were selected and fragmented by higher energy collisional dissociation. MS/MS spectra were acquired with a resolution of 15,000 (FWHM), at a maximum injection time of 50 ms, and a target value of 1e5 charges.

MS data analysis

Raw data was processed using MaxQuant version 1.5.0.25 with a false discovery rate (FDR) of 0.01 for peptides and proteins. MS/MS peaks were searched against the Uniprot reference proteome list of either *Caenorhabditis elegans* or *Homo sapiens*. Cysteine carbamidomethylation was set as a constant modification, whereas methionine oxidation and N-terminal acetylation were selected as variable modifications. Depending on the experiment, the match-between-run option was enabled and proteins were quantified using the label-free quantification (LFQ) algorithm. LFQ values were further processed using the Perseus software.

mRNA pulldown

3′-Biotin-TEG 20 nt antisense oligonucleotides targeting the coding region of YFP were designed as previously described with modifications.[115] Briefly, one probe per ~75 nt RNA length was designed with a target GC% of ~45%. Each oligo (listed in key resources table) was around 20 nt in length. Probes were adjusted to a final concentration of 100 μM (10 μM each). For immunoprecipitation,[43] standard nematode growth medium (NGM) plates were seeded with 300 μl of an overnight OP50 bacteria culture. The bacterial lawn was grown for 4-6 days before 20 L4 hermaphrodites were transferred. Worms were cultured at 20°C and monitored till the bacterial lawn was fully consumed (6-7 days). The plates were washed with M9 buffer and synchronized worms were transferred to 500 mL S-Basal. The culture was grown for 3 days with shaking at 120 rpm at 20°C. Worms were pooled in 50 mL Falcon tubes and washed several times with M9 buffer. The worm suspension was then transferred to unseeded 15 cm plates and exposed to 254 nm UV light (1J/cm^2) using a Stratalinker 1800 to crosslink interactions of RNA with proteins. The worm pellet was washed with lysis buffer (25 mM HEPES-KOH pH 7.4, 100 mM KoAC, 10 mM $MgCl_2$, 0.5 mM DTT, 2 tablets EDTA free protease inhibitor, 0.1 U/μL SUPERase*In) and frozen by dripping small droplets into liquid nitrogen.

Frozen worms were lysed using a Retsch Cryomill MM400 at 30 Hz (3 times 90 s with cooling between cycles). Lysate was thawed on ice and clarified at 2000 x g for 10 min at 4°C. Samples were adjusted to a concentration of 10 mg/ml protein and 250 pmol of probe (see key resources table) was added per 100 mg protein. Formamide was added to a final concentration of 7.5% and samples were incubated at 20°C by vertical rotation for 2 h. 200 μL of Dynabeads MyOne Streptavidin C1 (Thermo Fisher Scientific) were added to the lysate and incubated for 1 h at 20°C. The beads were washed 5 times and mRNA-bound proteins were digested on-bead using trypsin using the iST 8x kit (PreOmics), followed by analysis by mass spectrometry.

CRISPR knockout cell lines

HEK293T cells were seeded at a density of 250,000 cells in a 12-well plate. After 24 h the cells were transfected with px459 v2 plasmids encoding gene specific sgRNAs.[116] At 48 h post transfection, DMEM containing 2 μg/ml puromycin was added to cells. 4-5 days after selection, surviving cells were passaged and tested for knockouts by immunoblotting. For generating GCN1 knockout monoclones, single cells were sorted into 96 well plates and individual colonies were screened by immunoblotting.

siRNA treatment

HEK293T cells were split at a density of 750,000 cells in a 6-well plate. After 24 h the cells were transfected with 100 pmol of ON-TARGETplus Human CNOT1 siRNA (Dharmacon) using Lipofectamine 3000 following the manufacturer's instructions. After 48 h post transfection, the cells were split into a 12-well plate (250,000 cells/well). 24 h later (72 h after siRNA transfection), the cells were transfected with the reporter plasmids using Lipofectamine 3000. The effects of siRNA-mediated knockdown on the reporters were assessed 24 h later (96 h after siRNA transfection), using flow cytometry (see below).

Flow cytometry

HEK293T cells were transfected with various reporter plasmids 48h prior to measurement using Lipofectamine 3000 following the manufacturer's instructions. 100,000 single cells per replicate were measured on a Thermo Scientific Attune NxT analyser, using lasers at 405 nm (mTurquoise2), 488 nm (EYFP), 561 nm (mScarlet). Representative histograms were generated using FlowJo (v.10), ratiometric analysis was done using custom scripts written in Matlab (2019b), as previously described.[117] Signal bleedthrough from the red and blue channels (mScarlet and mTurquoise2, respectively) into the green channel (EYFP) was calculated using an 'RedBlue' control expressing a mScarlet and mTurquoise2 dual-CMV plasmid. Likewise, signal spillover from green and red channels (EYFP and mTurquoise2, respectively) was accounted for by expressing a 'GreenBlue' control (YFP and mTurquoise2 dual-CMV plasmid). The signal bleeding effects were subtracted before additional calculations.

Aggregate fractionation

HEK293T cells were washed with PBS and transferred to 1.5 ml tubes. The cells were counted and 10^6 cells pelleted by centrifugation at 400 x g for 3 min at 4°C. The cell-pellet was resuspended in 200 μl RIPA (Thermo) buffer and incubated for 20 min on ice, followed by sonication using a Biorupter (Diagenode) (7 cycles of 30 s with 30 s pause between cycles) at 4°C. The same number of cells was analyzed as input control. The cell lysate was then transferred to 0.5 ml open-top thickwall polycarbonate tubes (Beckman, #343776) and centrifuged at 100.000 x g for 1h at 4°C in a TLA-120.1 rotor (Beckman, #362224). The supernatant was transferred to a 1.5 ml

tube and the pellet was resuspended in 250 µl 1x HU buffer (8 M urea, 5% SDS, 200 mM Tris-HCL pH 6.8, 1 mM EDTA, 0.01% bromphenol blue, 2% β-mercaptoethanol). The supernatant and input were TCA-precipitated and resuspended in 250 µl 1x HU buffer for subsequent immunoblot analysis.

Protein pulldown

Worms were prepared as described for the mRNA pulldown and lysed in lysis buffer (25 mM HEPES-KOH pH 7.4, 100 mM KoAC, 10 mM $MgCl_2$, 0.5 mM DTT, 2 tablets EDTA free protease inhibitor) using a Biorupter (Diagenode). The lysate was clarified by centrifugation at 2000 x g for 10 min at 4°C. For each sample, 50 µl of GFP-Trap Magnetic Agarose beads (Chromotek) were prepared by washing the beads twice in 1 ml lysis buffer. Worm lysate (50 mg protein total) was adjusted to 10 mg/ml and added to the equilibrated beads. The suspension was then incubated for 2 h at 4°C with vertical rotation. The beads were washed once with 2 ml of lysis buffer and twice with 1 ml lysis buffer containing 0.1% NP-40. After transferring the beads to a fresh 1.5 ml tube, the beads were washed 3 times with lysis buffer without detergent. The bound protein was digested on beads using the iST 8x Kit (PreOmics) following manufacturer's instructions.

Preparation of total protein extracts for immunoblot analysis

Synchronized D1 adult worms were collected in M9 and OP50 bacteria were washed off with water until the supernatant was clear. Excessive water was aspirated without disrupting the worm pellet and an equal amount of lysis buffer was added (25 mM HEPES-KOH pH 7.4, 100 mM KoAC, 10 mM $MgCl_2$, 0.5 mM DTT, 2x EDTA free protease inhibitor). Nematodes were lysed by sonication in a Biorupter (Diagenode) as above. The lysate was clarified by centrifugation at 2,000 x g and the supernatant transferred to a fresh tube. Protein concentration was estimated by Bradford assay and adjusted to 1 mg/ml. 100 µl lysate was transferred to a fresh tube and 4 µl of 0.5% Na-deoxycholate was added. After 15 min incubation on ice, 10 µl of 100% TCA was added, followed by incubation for another hour on ice. The sample was centrifuged at 18,000 x g at 4°C for 30 min and the supernatant was discarded. The pellet was washed with 700 µl of ice-cold acetone and centrifuged for another 10 min at 18,000 x g at 4°C. The pellet was air dried and resuspended in 100 µl of 1x HU buffer (8 M urea, 5% SDS, 200 mM Tris-HCL pH 6.8, 1 mM EDTA, 0.01% bromphenol blue, 2% β-mercaptoethanol).

Total RNA isolation

Worms were synchronized by bleaching and grown up to D1 adult stage. The nematodes were then washed off the plate with M9 buffer and transferred to a 1.5 ml tube. Following 3 washes with M9 and 1 wash with water, 5 pellet volumes of TRIzol reagent (Invitrogen) was added. The worms were lysed by 3 cycles of freezing in liquid nitrogen (30 s) and thawing at 37°C. The suspension was then vortexed and left at RT for 5 min. Afterwards, 1 pellet volume of chloroform was added and the reaction shaken vigorously. After centrifugation at 12.000 x g for 15 min at 4°C the supernatant was transferred to a fresh tube and the RNA was precipitated using 2.5 volumes isopropanol. The pellet was washed in 70 % ethanol and air dried. Finally, the pellet was resuspended in RNAse-free water.

Quantitative real-time PCR

A quantity of 500 ng RNA was used for reverse transcription using random primers according to the manufacturer's protocol (Qiagen Quantitect Reverse Transcription Kit). qPCR reactions on cDNA contained Power SYBR green master mix (Applied Biosystems). Relative mRNA levels were determined using the ΔΔCT method, normalizing to *pmp-3* and *tba-1*.[118] For YFP quantification, results were normalized to the copy number using gDNA for each qPCR against YFP, normalizing to *tba-1*.

mRNA sequencing

mRNA sequencing libraries were prepared with 200 ng or 1 µg of total RNA of each sample using the NEBNext Ultra™ II Directional RNA Library Prep Kit for Illumina® (E7765, NEB) with NEBNext® Poly(A) mRNA Magnetic Isolation Module (E7490, NEB), according to standard manufacturer's protocol. Quality control of total RNA input and final libraries were performed using the Qubit™ Flex Fluorometer (Q33327, Invitrogen) and 4200 TapeStation System (G2991BA, Agilent). Paired-end sequencing was performed on an Illumina NextSeq 500. The samples were multiplexed and sequenced on one High Output Kit v2.5 to reduce a batch effect. BCL raw data were converted to FASTQ data and demultiplexed by bcl2fastq Conversion Software (Illumina).

Preparation of total ribosome fraction for ribosome profiling

C. elegans

Synchronized nematodes were transferred to 1 l S-Basal and grown in liquid culturentil D1 of adulthood or until D6, when indicated. FUdR (200 µM) was added when the culture had reached the L4/young adult stage. After thorough washing in M9, the nematodes were frozen in lysis buffer (25 mM HEPES-KOH pH 7.4, 100 mM KoAC, 10 mM MgCl2, 0.5 mM DTT, 2x EDTA free protease inhibitor, 0.1 U/µL SUPERase*In, 100 µg/mL cycloheximide) by dropwise transfer into liquid nitrogen. The nematodes were lysed with a Retsch Cryomill MM400 at 30 Hz for 3 times 90 s with cooling between cycles. The lysate was cleared for 10 min at 20,000 x g and 4°C. Ribosome protected fragments (RPFs) were recovered, and libraries were prepared as previously described.[60] Briefly, regions of 17-34 nt were excised from a 15% TBE-urea gel. The recovered RNA fragments were dephosphorylated with T4 PNK (NEB, M0201S) and ligated to a DNA barcoded linker using T4 Rnl2(tr) K227Q (NEB, M0351L). Non-ligated linkers were removed using yeast

5′-deadenylase and RecJ. rRNA depletion was performed using riboPOOL (siPOOLs) following the manufacturer's instructions. Reverse transcription was performed using Protoscript II reverse transcriptase (NEB, M0368L). Ligation products were excised from a 15% TBE-urea polyacrylamide gel after hydrolyzing the RNA template with NaOH (100 mM). Recovered ligation products were circularized using CircLigase I (Biozym, 131401) at 60°C for 2 h. Final libraries were generated by PCR amplification of the circularized cDNA template with Phusion polymerase (NEB, M0530L) using 6-14 cycles. Libraries were excised from a 8% TBE polyacrylamide gel and sequenced on an Illumina NextSeq 500 or NovaSeq 6000 system.

HEK293T cells

HEK293T cells were seeded into 15 cm plates 24 h prior to treatment. The cells were treated with 10 nM CC-885 and 20 μg/ml G418 for 4 h. Ribosome protected fragments (RPFs) were recovered, and libraries were prepared[60] as described above.

Preparation of ribosome fractions for GCN-1 selective ribosome profiling

C. elegans

The procedure for immunoprecipitation (IP) of GCN-1 bound ribosomes was adapted from.[59] Nematodes were synchronized by bleaching. L1 larvae were transferred to 1 L S-Basal. The animals were harvested at D1 of adulthood. Bacteria were removed by repeated washes in M9. In the last washing step, M9 was replaced by lysis buffer (25 mM HEPES-KOH pH 7.4, 100 mM KoAC, 10 mM $MgCl_2$, 0.5 mM DTT, 2x EDTA free protease inhibitor, 0.1 U/μL SUPERase*In, 100 μg/mL cycloheximide). After a quick spin, the worms were flash frozen in liquid nitrogen. The frozen worms were lysed with a Retsch cryomill MM400 at 30 Hz as above. The lysate was thawed on ice and clarified by centrifugation at 4,000 x g for 10 min at 4°C. Protein concentration was determined by Bradford assay. The supernatant fraction (80 mg of total protein) was partially digested with 3 units per 1 mg RNA RNase I (Epicenter) at 4°C for 1 h. Ribosomes were pelleted through a sucrose cushion (1 M, 20 U/mL SUPERase*In (Invitrogen)) at 55.000 rpm in a SW 55 Ti rotor (Beckman Coulter) for 2 h at 4°C and resuspended in lysis buffer supplemented with 10% glycerol. The IP was performed at 4°C for 1 h using M2 anti-FLAG magnetic agarose beads (Invitrogen). The beads were washed 10 times with lysis buffer and bound material was digested with 12.5 units of RNase I (Epicenter) at 23°C for 45 min (strong RNase I treatment). Ribosome protected mRNA fragments were eluted by adding TRIzol reagent (Invitrogen). For disome analysis the sizes between 54 to 68 nt were excised from the gel, using oligo markers previously described (see key resources table).[55] Monosome and disome libraries were prepared as described above[60] and sequenced on an Illumina NextSeq 500 or NovaSeq 6000 system.

HEK293T cells

Cells (treated with CC-885 or untreated) were harvested, washed with PBS and lysed by trituration through a 26 G needle for 10 times in lysis buffer (20 mM Tris, pH 7.4, 150 mM NaCl, 5 mM $MgCl_2$, 1 mM DTT, 100 μg/ml cycloheximide, 1 % Triton-X 100). The lysate was cleared at 4,000 x g for 10 min and an equivalent of 5 mg RNA input was digested with 15 units of RNAse I. The digested lysate was then layered over a sucrose cushion (1 M, 20 U/mL SUPERase*In (Invitrogen)) and centrifuged at 55.000 rpm in a SW 55 Ti rotor (Beckman Coulter) for 2 h at 4°C. The pelleted ribosomes were resuspended in lysis buffer supplemented with 10 % glycerol and incubated with GCN1 antibody (A301-843A, Thermo Fisher) coupled to protein G Dynabeads (10003D, Invitrogen) (5 μg antibody per 50 μl of protein G beads) for 2 h at 4°C. The beads were washed 10 times and digested with 4 units RNAse I for 45 min at 23°C. RPFs were isolated by TRIzol and libraries were prepared as described above.[60]

SLAM-seq

mRNA libraries for SLAM-seq analysis were prepared using the SLAM-seq Kinetics Kit (Lexogen), following the manufacturer's instructions. Briefly, to label the pre-existing mRNA, HEK293T cells were incubated with 100 μM 4sU for 24 h, changing the media every 3 h, keeping the cells in the dark. At the onset of the chase, the 4sU-containing media was removed and changed to media supplemented with 10 mM UTP (100x excess over 4sU). The cells were collected at timepoints 0, 2, 4, and 8 h after the onset of the chase. The library preps were performed using the QuantSeq 3'mRNA-seq kit (Lexogen). All subsequent steps during library preparation were performed under red light to avoid crosslinking. Libraries were sequenced on a NovaSeq 6000 system and the data processed using the SLAM-dunk pipeline.[84]

Polysome gradient analysis

Sucrose density gradients (10% - 50%) were prepared in SW41 ultracentrifuge tubes (Steton) using a BioComp Gradient Master (BioComp Instruments) according to manfucaturer's instructions. The individual 10% and 50% sucrose solutions were prepared in polysome buffer (20 mM Tris, pH 7.4, 150 mM NaCl, 5 mM $MgCl_2$, 1 mM DTT, 100 μg/ml, 20 U/ml SUPERase*In). The lysate concentration was assessed by Bradford assay and a total protein amount of 5 mg was loaded onto the gradients. The gradients were centrifuged for 2 h at 40,000 rpm at 4°C. The gradients were fractionated using a piston gradient fractionator coupled to an A254 nm spectrophotometer (Biocomp). Polysome fractions were pooled and precipitated using 10% TCA. The protein pellets were processed for mass spectrometry using the iST 8x kit (PreOmics) following the manufacturer's protocol.

SDS-PAGE

Proteins were separated on NuPAGE 4%–12% Bis-Tris SDS gels (Invitrogen) using NuPAGE MOPS SDS running buffer (Invitrogen) or NuPAGE MES SDS running buffer (Invitrogen) at 120 V for 1.5 h.

Microscopy

Worms were picked from plates, placed on 4% agarose pads and immobilized using polystyrene beads and a coverslip. Images for 3 color analysis were obtained using a Zeiss Axio Zoom.V16 microscope equipped with filtersets 46 (YFP), 47 (CFP) and 63 (RFP) and a Hamamatsu Orca Flash 4.0 camera. Confocal fluorescence images were obtained with an Olympus (Tokyo, Japan) FV1000 confocal microscope setup equipped with an Olympus PLAPON 60×/NA1.42 oil immersion objective or on a Leica SP8 FALCON confocal laser scanning microscope equipped with a LEICA HC PL APO 63x/NA 1.4 oil immersion objective. YFP was excited at 488 nm and emission detected at 505–540 nm. For red fluorophores, an excitation wavelength of 559 nm was used and emission detected at 575–675 nm. Images were visualized using Fiji.

Image analysis

Expression of 3-color reporter constructs for hydrophilic or hydrophobic 3′UTR fusion proteins was assessed in young (D0) nematodes. Fluorescence microscopy images of either YFP:mScarlet (protein) or mScarlet:CFP (mRNA/translation) were analyzed using a custom Fiji script. Briefly, the mScarlet channel was used to outline the muscle cells of the worm. Next, the channel intensities (pixel-wise) within the selected region were extracted. Pixels below an intensity threshold of 200 were excluded from downstream analysis. Linear regression analysis was applied to values of each pixel (for the corresponding channel). The resulting slope was used to express the ratios (normalized to respective STOP controls) depicted in the final data representation.

Analysis of ribosome profiling and mRNA-seq data

Sequencing reads were demultiplexed and trimmed using a custom awk script. The UMI were extracted using UMI-tools using the option '–extract-method=regex –bc-pattern="(?P<umi_1>.{2}).+(?P<umi_2>.{6})$"', which serves to remove duplicated reads arising from library amplification. The clipped reads were then mapped against ncRNA/rRNA indices using Bowtie2 (v2.4.2) with the parameters '-N 1 -L 15'. Unaligned reads were mapped against the genome using STAR (v2.7.10a) with parameters '–outFilterMismatchNmax 2 –quantMode TranscriptomeSAM GeneCounts –outSAMattributes MD NH –outFilterMultimapNmax 1'. The P-site offset and metagene plots were computed using the R package "riboWaltz."[119] Transcript enrichment was calculated with the R package "DESeq2"[120] or "DEBrowser."[74] Enrichment plots around the first TMD, pause scores, tAI scores and A-site occupancy (using offsets calculated with riboWaltz) were computed using "RiboMiner."[121] For disomes the A-site offset was assigned to the leading ribosome using the stop codon peak for the offset calculation. Pause scores are defined as the sum of normalized ribosome densities (AU) on each tripeptide motif. Motifs with a pausing score of < 5 (low confidence) in aged wild-type animals were excluded from downstream analysis. Read count matrices of reads mapping into the 3′UTRs of transcripts were generated using featureCounts (v2.0.1)[122] (Figure S5B). Metagene plots around polyproline stretches were analyzed as previously described.[5] Briefly, reads were aligned at the A-site around the onset of the polyproline stretch. The polyproline stretch was defined as a 12 amino acid window with at least 8 of the 12 residues being proline. Next, the mean was calculated and the 95% confidence intervals at each position. Transcripts with average reads per codon within the analyzed window of less than 0.5 were discarded. mRNA half-lives were calculated as described.[123] Briefly, T>C conversions were normalized to the chase-onset. Curve fitting (non-linear regression) was performed in R using the minpack.lm package. Only RNAs that met an $R^2 > 0.6$ (goodness of fit) cutoff were used for downstream analysis. Codon stability coefficients (CSC) were calculated as the Pearson's correlation coefficient between codon content and mRNA half-lives. Similarly, codon recruitment coefficients (CRC) were calculated as the Pearson's correlation coefficient between codon occurrence and GCN-1 recruitment.

QUANTIFICATION AND STATISTICAL ANALYSIS

Preparation of graphs and statistical analyses were performed using GraphPad Prism 8 or R(4.1.0). The statistical tests applied are indicated in the corresponding figure legends. For multiple comparisons, one- and two-way ANOVA were used with the following corrections: Dunnett and Holm-Sidak. When two groups were compared, statistical significance was computed using Student's t-tests and Mann-Whitney tests. *P*-Values < 0.05 were considered significant.

Supplemental figures

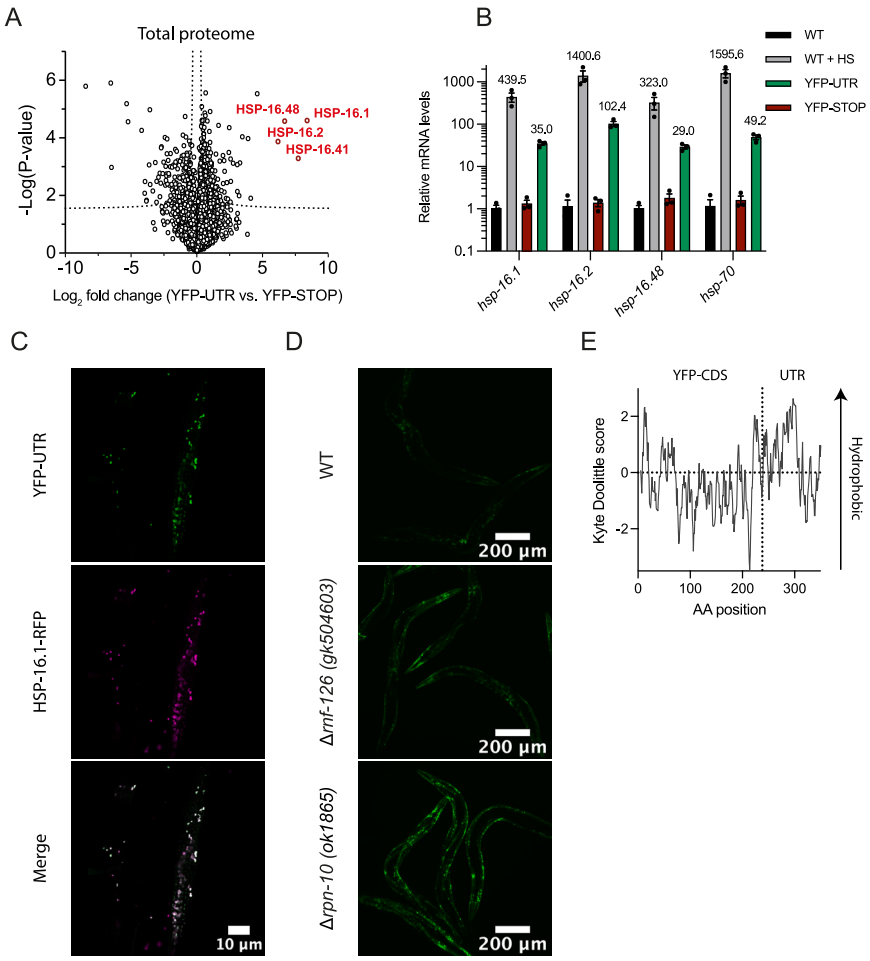

Figure S1. Characterization of readthrough quality control machinery, related to Figure 1

(A) Readthrough into 3′ UTR induces expression of sHSPs. Volcano plot representation of label-free proteome analysis of YFP-UTR and YFP-STOP expressing nematodes. sHSPs are highlighted in red. See Table S1K.

(B) Relative mRNA levels (qPCR analysis) of *hsp-16* family members and *hsp-70* (C12C8.1) in animals (day 0) expressing YFP-UTR. Wild-type (WT) nematodes (untreated or exposed to heat stress [HS]) and animals expressing YFP-STOP were analyzed as controls. HS was performed for 60 min at 34°C. Error bars represent mean ± SEM (n = 3).

(C) Expression of readthrough reporter protein in *C. elegans* muscle cells in the presence of a HSP-16.1-RFP reporter. Representative fluorescence microscopy images of animals expressing YFP-UTR are shown.

(D) YFP-UTR undergoes proteasomal degradation. Representative fluorescence microscopy images of wild-type, Δ*rnf-126*, and Δ*rpn-10* worms expressing YFP-UTR. (Exposure 200 ms, 100× magnification.)

(E) Hydrophobicity analysis of YFP-UTR using Kyte Doolittle scores (KDSs) as metric. AA, amino acid.

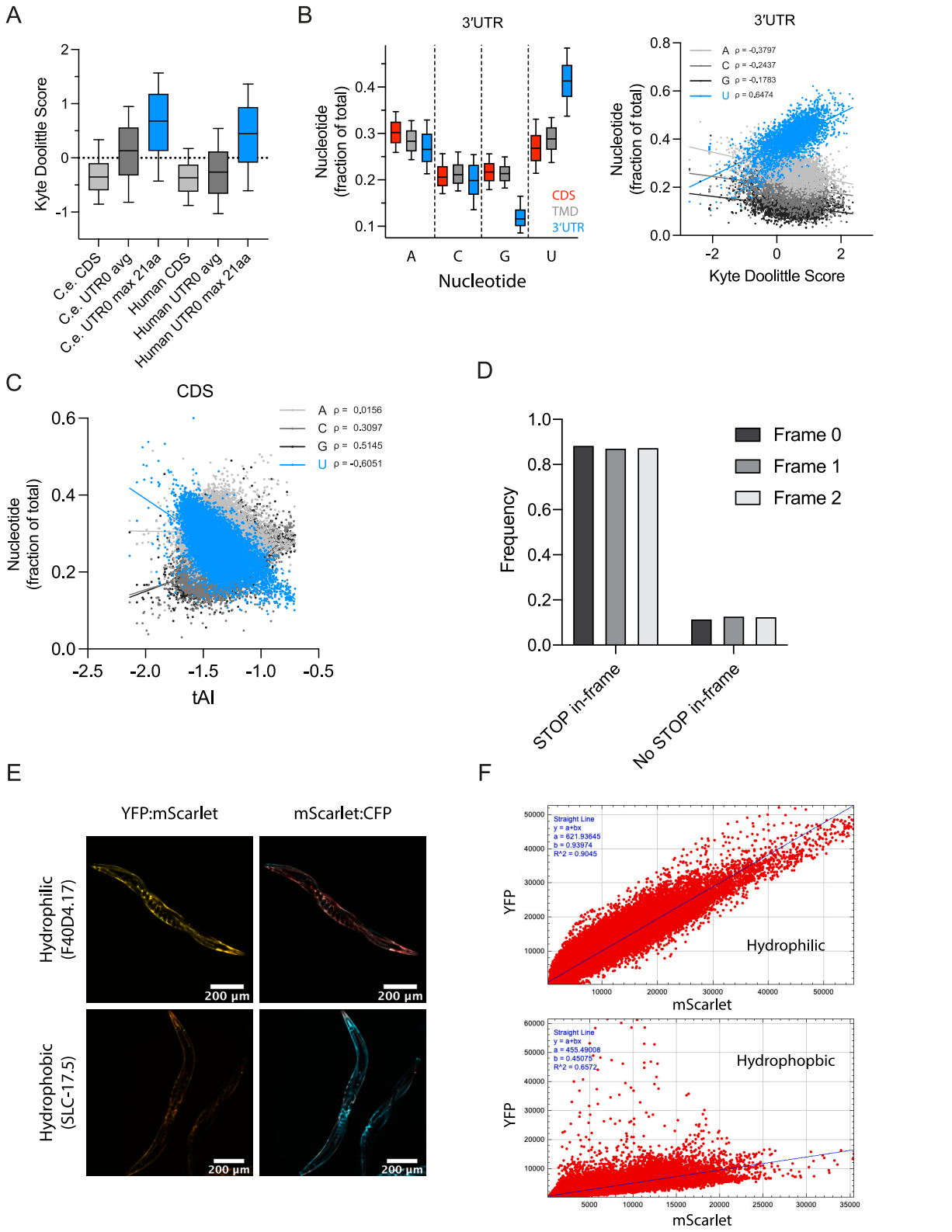

Figure S2. Sequence features of *C. elegans* 3′ UTRs, related to Figure 2

(A) Boxplots of Kyte Doolittle scores indicating hydrophobicity of CDS regions, 3′ UTRs and maximum hydrophobicity score (max. score) of a 21AA window (average TA length) within 3′ UTRs in *C. elegans* and human.

(legend continued on next page)

(B) Relationship of nucleotide composition and sequence properties. Left: nucleotide composition in *C. elegans* of coding sequences (CDSs), red; TMD transcripts, gray; 3′ UTRs, blue. Right: correlation of 3′ UTR nucleotide composition and hydrophobicity of their translated peptides. U-content positively correlates with hydrophobicity in *C. elegans*.

(C) Correlation analysis of nucleotide composition and tAI score indicates a negative correlation between U-content and codon optimality.

(D) Occurrence of in-frame stop codons in 3′ UTRs. 3′ UTRs typically contain at least one stop codon before the poly(A) tail (~90%) in all three reading frames.

(E) Expression of 3-color reporter constructs for either hydrophilic (top) or hydrophobic (bottom) 3′ UTR fusion proteins. Representative fluorescence microscopy images (overlay) of either YFP:mScarlet (left, ratio of YFP to mScarlet) or mScarlet:CFP (right, ratio of mScarlet to CFP) channels are shown.

(F) Representative ratiometric analysis of YFP by mScarlet ratios performed on images shown in (D). The mScarlet channel was used to outline the muscle cells expressing the reporter construct. Linear regression analysis was applied to values of each pixel (for the corresponding channel). The resulting slope was used to express the ratios depicted in Figures 2E, 2F, 3D, and 3E.

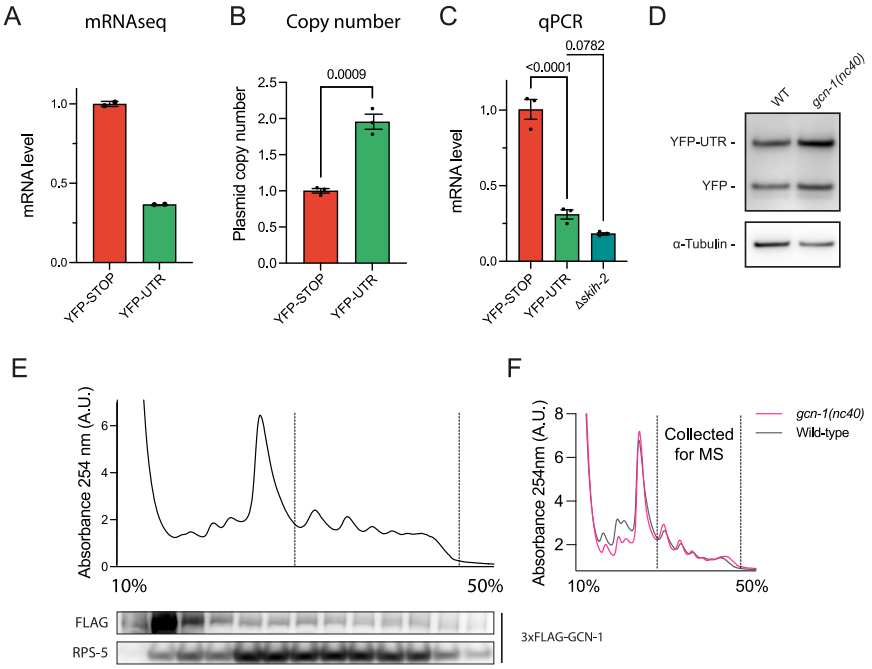

Figure S3. Effects of 3′ UTR translation on mRNA and protein levels, related to Figure 3

(A) mRNA-seq analysis of *C. elegans* reporter strains expressing YFP-UTR and YFP-STOP (n = 2). Error bars represent mean ± SEM.

(B) qPCR analysis of copy number of YFP-UTR and YFP-STOP in *C. elegans* reporter strains. Integrated gene copy numbers are on average 1.96 ± 0.11-fold higher in YFP-UTR compared with YFP-STOP. Error bars represent mean ± SEM (n = 3). Data were analyzed using the $2^{(-\Delta\Delta Ct)}$ formula. p values by unpaired t test.

(C) qPCR analysis of YFP-STOP and YFP-UTR mRNA levels in wild-type *C. elegans* and in *skih-2* mutant animals. Error bars represent mean ± SEM (n = 3). Data were analyzed using the $2^{(-\Delta\Delta Ct)}$ formula. p values by Fisher's LSD test.

(D) Representative immunoblot analysis of wild-type or *gcn-1(nc40)* mutant worms expressing YFP-UTR. See Figure 3C for quantification.

(E) Representative trace of sucrose density gradient fractionation ($A_{254\ nm}$; top) and immunoblot analysis of 3x-FLAG-tagged GCN-1 in *C. elegans*. Dotted lines delineate polysome fractions.

(F) Representative traces of sucrose gradient density fractionation of wild-type and *gcn-1(nc40)* mutant animals ($A_{254\ nm}$). Dotted line indicates polysomes collected for subsequent MS/MS analysis shown in Figures 3G and 5E.

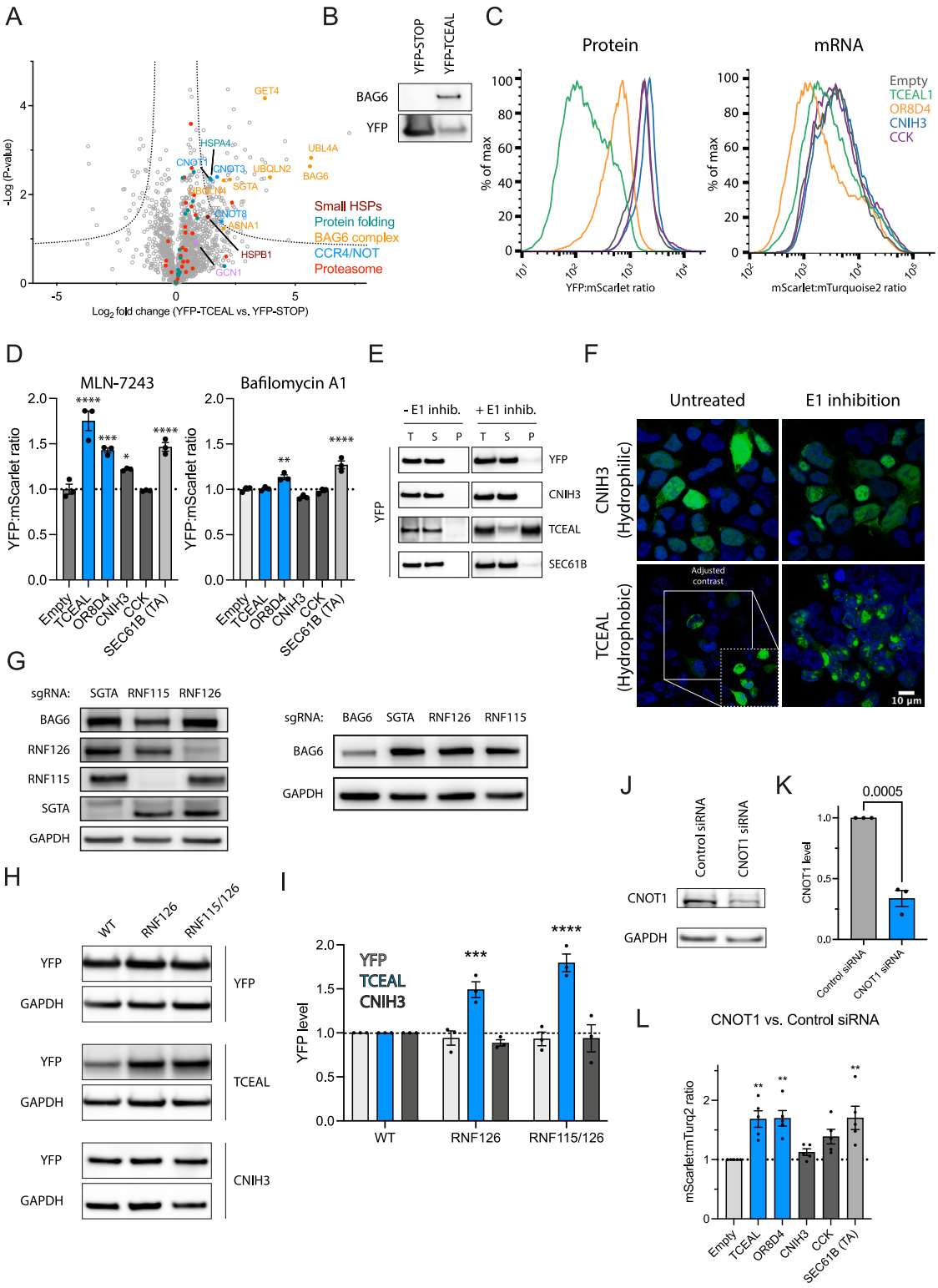

Figure S4. Protein and mRNA clearance upon translational readthrough is conserved in HEK293T cells, related to Figure 4

(A) Volcano plot representation of label-free interactome analysis of YFP-TCEAL from HEK293T cells expressing YFP-TCEAL CTE construct and YFP-STOP as control. Components of the BAG6, proteasomal subunits, heat-shock proteins (e.g., HSPB1 and HSPA4) and CCR4/NOT complexes are identified as interactors of YFP-TCEAL. Selected proteins are highlighted. See also Table S1L.

(legend continued on next page)

(B) Immunoprecipitation of YFP-STOP or YFP-TCEAL with anti-GFP antibody from HEK293T cells expressing the respective constructs. Fractions were analyzed by immunoblotting for BAG6 and YFP (n = 2). Note that the UTR sequence adds 30 amino acids (mainly hydrophobic) to the C terminus of YFP, resulting in only slightly slower migration of YFP-TCEAL compared with YFP-STOP.
(C) Representative histograms of flow cytometry analysis indicating YFP:mScarlet and mScarlet:mTurquoise2 ratios of cells transiently transfected with the indicated reporter plasmids (related to Figures 4B–4D).
(D) Ratiometric flow cytometry analysis of cells expressing the indicated reporter plasmids (see Figure 4A) in the presence of the E1 ubiquitin-activating inhibitor MLN-7243 (compared with untreated cells) (n = 3; left) and the lysosomal degradation inhibitor bafilomycin A1 (compared with untreated cells) (n = 3; right). Error bars represent mean ± SEM. p values by Dunnett's test. *$p < 0.05$; **$p < 0.01$; ***$p < 0.001$; ****$p < 0.0001$.
(E) Representative immunoblot analysis of soluble and pellet fractions from cells expressing the indicated reporter constructs (see Figure 4A). YFP-TCEAL is recovered in the pellet fraction upon E1 inhibition.
(F) Representative fluorescence microscopy images of hydrophobic (YFP-TCEAL) or hydrophilic (YFP-CNIH3) readthrough reporter proteins with or without E1 inhibition by MLN-7243. Insert in the lower left image shows cells after contrast adjustment for the low expression level of the YFP-TCEAL readthrough reporter.
(G) Representative immunoblot analysis of HEK293T depletion cell lines for components of the BAG6 complex.
(H) Representative immunoblot analysis of reporter constructs in different BAG6 mutant backgrounds shown in (F). Related to Figure 4D.
(I) Quantification of immunoblot analysis in (G) by densitometry (n = 3). p value by Dunnett's test. Error bars represent mean ± SEM. ***$p < 0.001$; ****$p < 0.0001$. Related to Figure 4D.
(J) Representative immunoblot analysis of downregulation efficiency using siRNA against CNOT1 compared with control siRNA. p value by unpaired t test.
(K) Quantification of immunoblot analysis in (I) by densitometry. Error bars represent mean ± SEM (n = 3). p value by Dunnett's test.
(L) Effect of downregulation of CNOT1 on mRNA level of 3′ UTR reporter constructs and SEC61B (TA). Ratiometric analysis by flow cytometry of cells treated with siRNA against CNOT1 or control siRNA. Error bars represent mean ± SEM (n = 5). p value by Dunnett's test. ***$p < 0.001$.

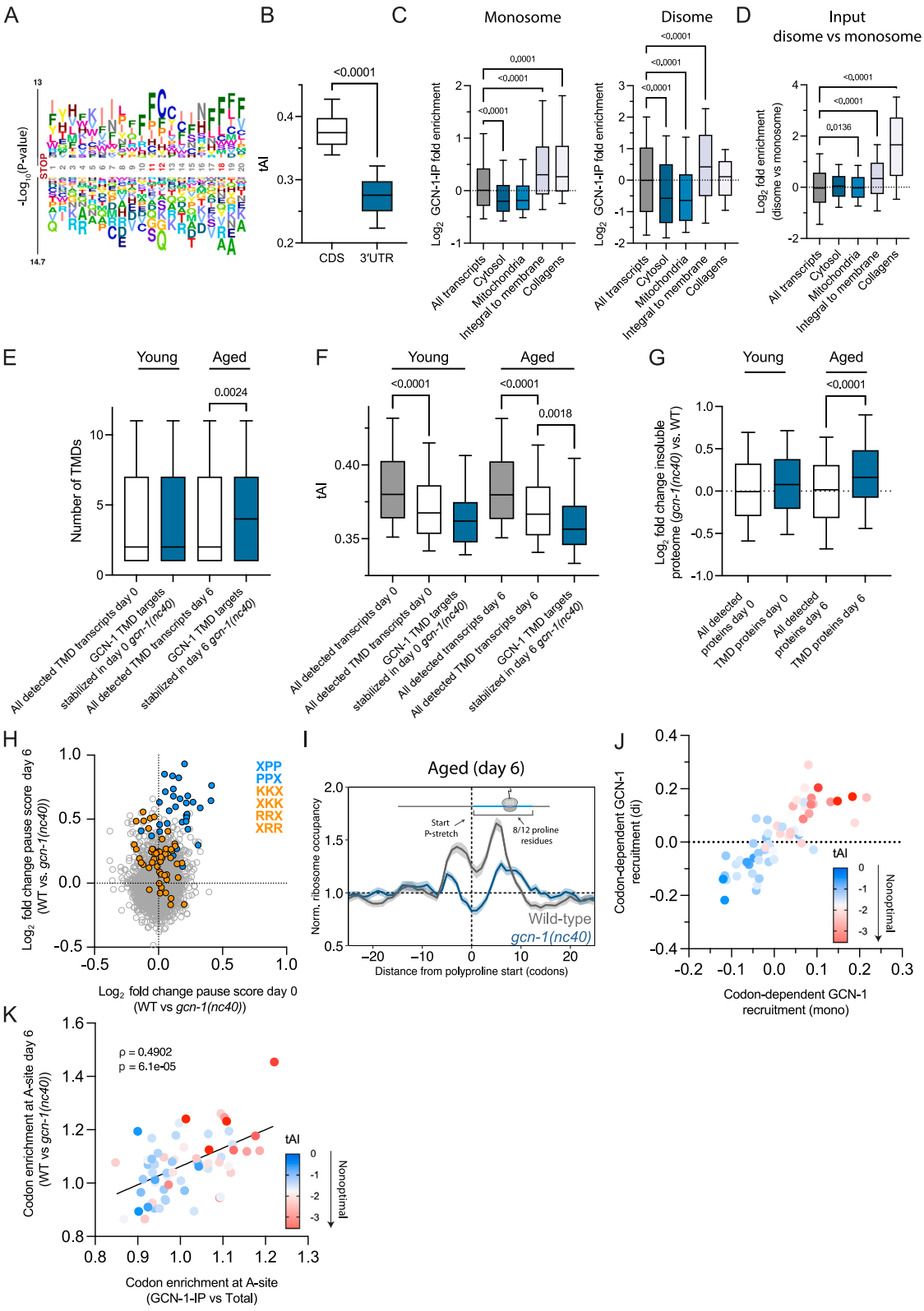

(legend on next page)

Figure S5. GCN-1 is recruited to ribosomes translating hydrophobic 3′ UTRs, TMD proteins, and collagens, related to Figure 5

(A) Logo plots of amino acid enrichment using kplogo analysis (Wu and Bartel[124]). Sequences (20 aa downstream of annotated stop codon) chosen for analysis were derived from 3′ UTRs bound by GCN-1 (monosomes and disomes; in frame 1) indicated in Figure 5A (right). Numbers indicate the position after the stop codon. The y axis indicates the sum of log p values for each amino acid at a given position. Significantly enriched positions are marked in red. Also see Table S2C.

(B) 3′ UTRs are enriched in nonoptimal codons. tRNA adaptation index (tAI) was analyzed for coding sequences (CDSs) (n = 20,190) and 3′ UTRs (n = 14,434) in *C. elegans*. The horizontal line in the boxplots indicates the median; boxes indicate upper and lower quartile and whisker caps 10^{th}–90^{th} percentile, respectively. p value by unpaired t test.

(C) GCN-1 recruitment (log_2 enrichment) across transcripts of proteins from different cellular compartments based on monosomes (left) (all transcripts, n = 12,894; cytosol, n = 432; mitochondria, n = 301; integral to membrane n = 2,158; collagens, n = 115) or disomes (right) (all transcripts, n = 16,294; cytosol, n = 590; mitochondria, n = 478; integral to membrane n = 3,838; collagens, n = 129). The horizontal line in the boxplots indicates the median; boxes indicate upper and lower quartile and whisker caps 10^{th}–90^{th} percentile, respectively. p values by Dunnett's test. See Tables S2D and S2E.

(D) Disome enrichment (log_2 enrichment) across transcripts of proteins from different cellular compartments (all transcripts, n = 15,036; cytosol, n = 584; mitochondria, n = 479; integral to membrane n = 5,733; collagens, n = 154).

(E) GCN-1 dysfunction preferentially stabilizes mRNA levels of integral membrane proteins with multiple TMDs in aged animals. This analysis depicts the number of TMDs that are encoded by GCN-1 target transcripts. These transcripts were defined as meeting two criteria: (1) having 2-fold enrichment by selective ribosome profiling and (2) displaying ~1.15-fold (log_2 0.2) stabilization in the *gcn-1(nc40)* mutant animals compared with wild type. The distribution of the TMD number in these GCN-1 target transcripts (blue) were compared with the TMD number in all transcripts (white) detected in our experiments in day-0 and day-6 animals. The horizontal line in the boxplots indicates the median; boxes indicate upper and lower quartile and whisker caps 10^{th}–90^{th} percentile, respectively. p value by Holm-Sidak's test. Also see Table S3C.

(F) TMD transcripts are enriched in nonoptimal codons. tAI analysis of all TMD transcripts (white), TMD transcripts stabilized in *gcn-1(nc40)* mutant nematodes (blue) in comparison with all coding sequences (CDSs, gray). Only transcripts that were detected in both mRNA-seq and GCN-1 selective ribosome profiling were considered for analysis matching the same criteria as in (E) for day-0 and day-6 animals (also see Table S3C). The horizontal line in the boxplots indicates the median; boxes indicate upper and lower quartile and whisker caps 10^{th}–90^{th} percentile, respectively. p value by Holm-Sidak's test. See Table S3C.

(G) Age-dependent effect on TMD protein insolubility in GCN-1-deficient (*gcn-1(nc40)*) nematodes. TMD proteins identified by mass spectrometry in the insoluble fraction of lysates from young (day 0) and aged (day 6) worms were analyzed. The log_2 fold increase in insolubility from day 0 to day 6 is shown. The horizontal line in the boxplots indicates the median; boxes indicate upper and lower quartile and whisker caps 10^{th}–90^{th} percentile, respectively. p value by Dunnett's test. See also Tables S1E–S1H.

(H) Age-dependent effect of GCN-1 dysfunction on translational pausing at tripeptide motifs. Translational pause scores were analyzed from ribosome profiling data for tripeptide motifs in young (x axis, day 0) and old (y axis, day 6) *gcn-1(nc40)* mutant animals compared with age-matched wild-type animals (n = 18,612 motifs). PP containing motifs are highlighted in blue and KK or RR motifs in orange. The pause score is calculated as the sum of normalized ribosome densities on each triplet amino acid motif. Only transcripts with at least 10 reads and a minimum length of 100 nt were considered for the analysis.

(I) Normalized ribosome occupancy (mean scaled) centered around onset of polyproline stretch (x = 0; dashed vertical line; with at least 8 out of 12 residues being proline) in aged (n = 192 positions from 142 genes) wild-type (gray) and *gcn-1(nc40)* (blue) animals. The light gray (wild type) and light blue (*gcn-1(nc40)*) shaded areas indicate the 95% confidence interval.

(J) Codon recruitment coefficients calculated as the Pearson's correlation coefficient of GCN-1 recruitment (monosomes [x axis] and disomes [y axis]) and codon frequency of transcripts reveal increased GCN-1 recruitment to nonoptimal codons. Codon optimality is represented as a color gradient from blue (optimal) to red (nonoptimal).

(K) Dysfunction of GCN-1 (in *gcn-1(nc40)* mutant) results in an age-dependent decrease of ribosome pausing at nonoptimal codons. Codon enrichment at A-site of GCN-1-IPed ribosomes relative to total input in (H) (x axis) is compared with codon enrichment at A-site of wild-type relative to *gcn-1(nc40)* mutant nematodes. Codon optimality (tAI) is indicated by color-scale (red, low codon optimality; blue, high codon optimality). Statistics by Spearman's correlation (ρ = 0.4902, p = 6.1e−5). Line represents linear regression fit.

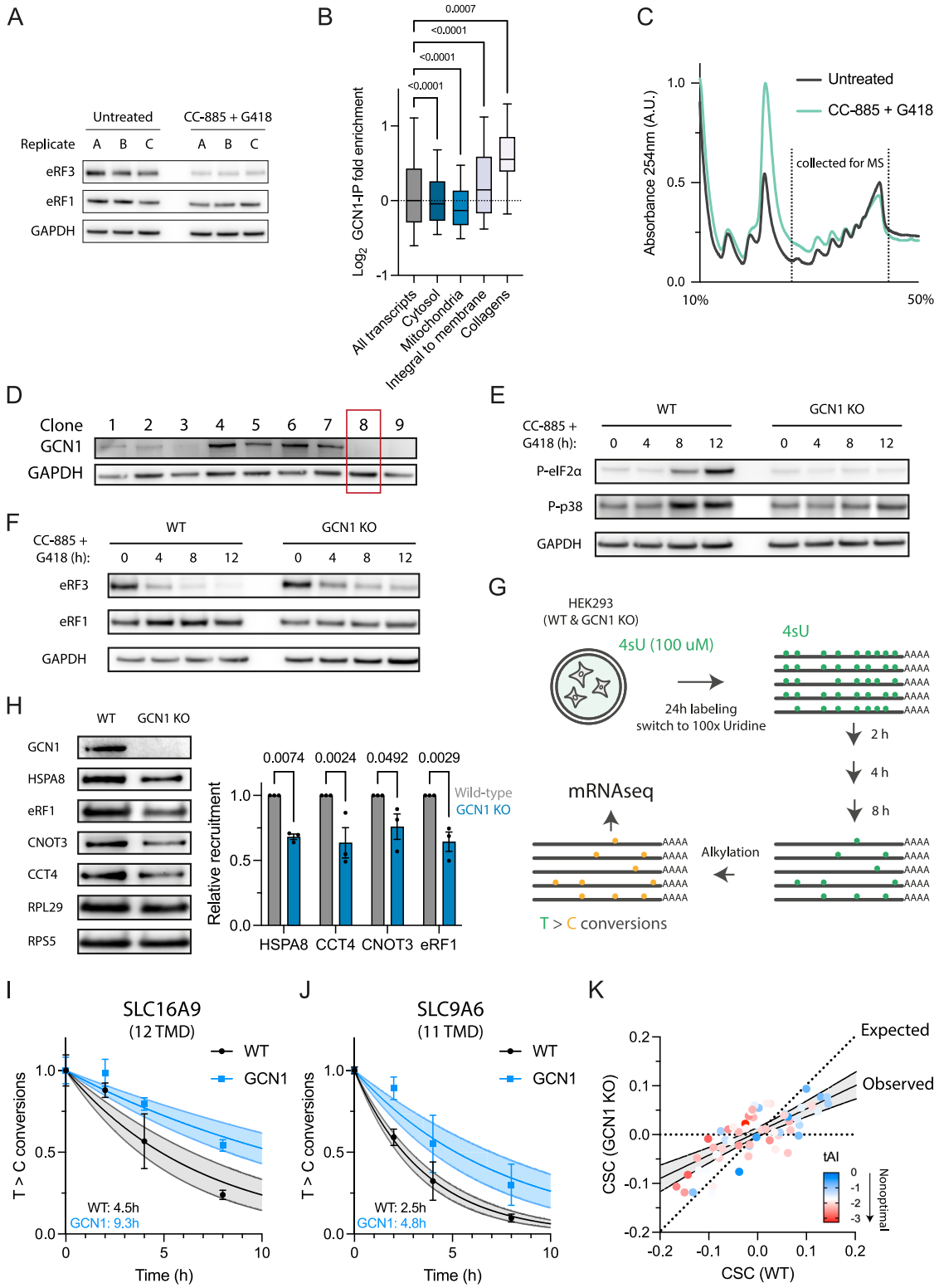

Figure S6. GCN1 function is conserved in HEK293T cells, related to Figure 6

(A) Immunoblot analysis of eRF3 upon treatment of HEK293T cells with CC-885 (10 nM) and G418 (20 μg/mL) for 4 h to induce readthrough (n = 3).

(B) GCN1 recruitment (log_2 enrichment) based on selective ribosome profiling in untreated HEK293T cells across transcripts of proteins from different cellular compartments (all transcripts, n = 16,246; cytosol, n = 4,488; mitochondria, n = 1,463; integral to membrane n = 3,301; collagens, n = 60). The horizontal line in the

(legend continued on next page)

boxplots indicates the median; boxes indicate upper and lower quartile and whisker caps 10^{th}–90^{th} percentile, respectively. p values by Dunnett's test. See Table S2G.

(C) Sucrose density gradient fractionation of HEK293T cells treated with CC-885 and G418 as in (A). The dotted lines delineate fractions collected for proteome analysis shown in Figure 6C.

(D) Immunoblot analysis of single-cell-sorted polyclonal GCN1 deletion cells. Clone 8 (red square) was chosen for the experiments in Figures 6D, S6D, and S6E.

(E) Representative immunoblot analysis of eIF2α and p38 phosphorylation during eRF3 depletion upon treatment of cells with CC-885 and G418 for the times indicated. Related to Figure 6D.

(F) Representative immunoblot analysis of eRF3 depletion upon treatment of wild-type and GCN1 KO cells with CC-885 and G418 for the times indicated. Related to Figure 6D.

(G) Schematic overview of SLAM-seq workflow. Preexisting mRNAs are labeled for 24 h with 4-thiouridine (4sU). Then the media is exchanged with 100X uridine-containing media, which marks the onset of the chase. Over time, the 4sU-labeled mRNAs will be degraded. The prelabeled mRNA can be distinguished from newly synthesized mRNA by alkylating the 4sU-labeled sites, leading to T > C conversions upon reverse transcription. The loss of T > C conversions over time allows the calculation of mRNA half-lives.

(H) Immunoblot analysis of ribosomes purified by centrifugation through a sucrose cushion with antibodies against GCN1, HSPA8, eRF1, CNOT3, CCT4, RPL29, and RPS5 (left). Blots were quantified by densitometry (right) (n = 3). Error bars represent mean ± SEM. p values by Holm-Sidak's test.

(I and J) (I) Examples of mRNA turnover profiles of two multipass TMD-encoding transcripts. SLC16A9, 12 TMD segments and (J) SLC9A6, 11 TMD segments. Each time point (0, 2, 4, and 8 h) is represented by dots, and error bars indicate SEM. The lines indicate nonlinear fits and the light-colored shaded area the 95% confidence intervals.

(K) Loss of GCN1 generally dampens codon dependence of mRNA turnover rates, which correlate with codon optimality, represented by a color gradient from blue (optimal) to red (nonoptimal) based on tAI scores. Dotted line indicates no difference in CSC between wild-type and GCN1 knockout cells. Solid line indicates observed change in CSC with shaded area representing the 95% confidence interval.